Politecnico di Torino

Master Dissertation

Synthesis and Characterization of Mesoporous doped Iron-Nitrogen-Carbon Catalysts for the Oxygen Reduction Reaction

By

Alireza Eghdami Malati

******

Supervisor(s):

Prof. Juqin Zeng

Co-tutors:

Prof. Candido Fabrizio Pirri

Dr. Giulia Gianola

Politecnico di Torino

2025 _ 2026

Abstract

The growing global demand forfglobally sustainable energy technologies has fueled the quest for efficient electrocatalysts for fuel cell applications. The oxygen reduction reaction (ORR) at the cathode remains a major kinetic limitation affecting the performance of proton exchange membrane fuel cells (PEMFCs). Currently, platinum-based catalysts have the highest ORR activity. Nevertheless, the high cost, scarcity, and long-term ORR activity of platinum-based catalysts remain major barriers to the large-scale commercialization of PEMFCs. As a result, there has been a notable quest for the synthesis of novel electrocatalysts from earth-abundant elements, among which the Fe-N-C catalysts have been noted for their desirable catalytic activity coupled with structural flexibility.

This chapter explains how the presence of heteroatom dopants affects the structural and electrochemical behavior of mesoporous Fe-N-C catalysts. Boron-doped (FeNBC) and sulfur-doped (FeNSC) catalysts, prepared using the hard-template synthesis method, were studied. The hard-template method involved the infiltration of iron, nitrogen, and carbon precursor materials into the ordered pores of an SBA-15 mesoporous silica template. The catalysts were produced by high-temperature pyrolysis of the precursor materials under a nitrogen atmosphere, followed by chemical removal of the silica template using sodium hydroxide (NaOH) and hydrochloric acid (HCl) to remove metallic species and impurities. The result of this process is that a mesoporous carbon material was created that has the same structure as the SBA-15 template. Before performing a second pyrolysis to increase graphitization, electrical conductivity, and stability, boron and sulfur dopants were incorporated into the precursor preparation (using boric acid and thiourea, respectively) to create catalysts with different levels of doping.

The produced materials were examined by Scanning Electron Microscopy (SEM) and Energy Dispersive X-ray Spectroscopy (EDX), determining morphology, structure, and elemental composition. The electrochemical testing of the catalysts was performed using a Rotating Disk Electrode (RDE) and Rotating Ring-Disk Electrode (RRDE) method, in order to investigate the catalytic activity of oxygen reduction reactions (ORR). The data show that the sulphur doped catalysts had superior ORR performance as compared to the boron doped catalysts. The catalyst doped with FeNSC presented an dopant of sulfur, and had electrochemical characteristics very similar to the reference sample of Fe-N-C, as exhibited by their close onset potential and limiting current density. Furthermore, the electrochemical results showed that all of the catalysts were predominantly four-electron ORR materials, with low yields of hydrogen peroxide, thereby exhibiting high catalytic efficiencies and selectivities for the ORR.

Results indicate that sulfur-doped catalysts maintain the templated mesoporous SBA-15 structure with a more uniform elemental distribution. Conversely, the boron-doped samples have less defined morphology and higher apparent boron content, which can be attributed to EDX quantification limitations arising from peak overlap with carbon. Collectively, this study has provided further understanding of the role of heteroatom doping in tuning the structural and electrochemical properties of Fe-N-C catalysts and will assist in developing low-cost electrocatalysts for use in fuel cells.

Table of Contents

1. INTRODUCTION 6

1.1 Global Energy Challenges and Fuel Cells 6

1.2 Oxygen Reduction Reaction in Fuel Cells 7

1.3 Catalysts for ORR: From Platinum to Fe-N-C Materials 10

1.4 Fe-N-C Catalysts: Structure, Performance, and Challenges 11

1.4.1 Active sites and catalyst structure 11

1.4.2 Main challenges: activity, conductivity, and durability 12

1.4.3 Strategy for Fe-N-C synthesis: the hard template method 12

1.5 Role of dopants to boost ORR performance in M-N-C electrocatalysts 13

1.5.1 Effect of boron doping on Fe-N-C catalysts 13

1.5.2 Effect of sulfur doping on Fe-N-C catalysts 14

1.6 Goal and outline of the thesis 14

2. MATERIALS AND METHODS 16

2.1 Materials and Chemicals 16

2.1.1 Chemicals and precursors used for catalyst synthesis 16

2.1.2 Gases and electrolytes for electrochemical measurements 17

2.2 Synthesis of the Hard Template (SBA-15) 17

2.2.1 Preparation of SBA-15 18

2.3 Synthesis of Fe-N-C Based Catalysts 19

2.3.1 Synthesis of Fe-N-C catalys 19

2.3.2 Boron-doped Fe-N-C catalysts 20

2.3.3 Sulfur-doped Fe-N-C catalysts 21

2.4 Electrode Preparation 21

2.4.1 Catalyst ink preparation 21

2.4.2 Drop-casting on glassy carbon 22

2.5 Electrochemical Characterization: RDE and RRDE 23

2.5.1 RDE and RRDE analysis 23

2.5.2 Electrochemical setup 25

2.5.3 Cyclic voltammetry and linear sweep voltammetry measurements 25

2.5.4 Trochemical impedance spectroscopy (EIS) measurements 26

2.5.5 Stability tests 26

2.6 Chemical and Physical Characterization Methods 27

2.6.1 Energy dispersive x-ray spectroscopy 27

2.6.2 Scanning Electron Microscopy (SEM) 27

3. RESULTS AND DISCUSSION : Physico-Chemical characterization 29

3.1 Energy dispersive x-ray spectroscopy (EDX) 29
3.2 Scanning Electron Microscopy (SEM) 31
4. RESULTS AND DISCUSSION : Electrochemical Characterization 34
4.1 Electrochemical Characterization: Rotating (Ring) Disk Electrode 34
4.2 Electrochemical Activity of Undoped Fe-N-C 34
4.2.1 Cyclic Voltammetry (CV) Analysis 34
4.2.2 Linear Sweep Voltammetry (LSV) Analysis 35
4.2.3 Oxygen Reduction Reaction (ORR) Pathway Analysis 37
4.2.4 Stability Test 38
4.2.5 Discussion 42
4.3 Electrochemical Activity of Undoped Fe-N-C vs Boron Doping Catalysts 44
4.3.1 Cyclic Voltammetry (CV) Analysis 44
4.3.2 Linear Sweep Voltammetry (LSV) Analysis 45
4.3.3 Oxygen Reduction Reaction (ORR) Pathway Analysis 48
4.3.4 Stability Test 50
4.3.5 Discussion 53
4.4 Electrochemical Activity of Undoped Fe-N-C vs Sulfur Doping Catalysts 55
4.4.1 Cyclic Voltammetry (CV) Analysis 55
4.4.2 Linear Sweep Voltammetry (LSV) Analysis 56
4.4.3 Oxygen Reduction Reaction (ORR) Pathway Analysis 59
4.4.4 Stability Test 61
4.4.5 Discussion 64
5. CONCLUSIONS 66
REFERENCES 69

CHAPTER 1

1. INTRODUCTION

1.1 Global Energy Challenges and Fuel Cells

Due to the continuous growth of the global population and the associated increase in industrial activities, global energy demand has risen significantly. Although the majority of energy production still relies on fossil fuels such as coal and petroleum, it is now well established that these resources cause severe environmental problems. The most critical of these issues are greenhouse gas (GHG) emissions, along with other pollutants, such as sulfur dioxide (SO_2), which are generated during combustion.[1]. As shown in Figure 1.1, fossil fuels still represent the dominant share of global primary energy consumption in 2024.

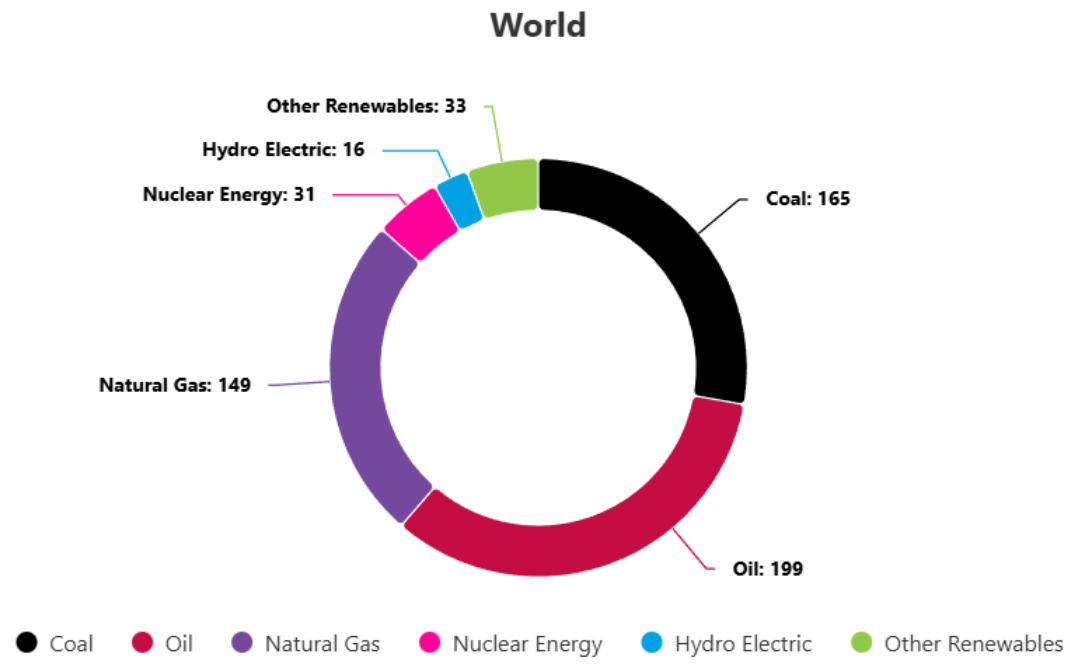

Figure1 -1 Global primary energy consumption by source in 2024 [2]

Carbon dioxide (CO_2), a significant GHG, is emitted primarily from fossil fuel combustion. Therefore, the importance of developing clean and renewable energy systems is consistently recognized as a means of addressing the problem of increasing levels of atmospheric carbon dioxide and other greenhouse gases.

In response to environmental degradation and increasing energy production and use, there has been a strong emphasis on developing new technologies for producing renewable forms of energy with reduced levels of GHG emissions while maintaining high-level efficiencies.

New technologies using both wind and solar sources of renewable energy have been identified as two of the most promising methods for producing renewable energy, yet they each have challenges associated with their use due to their lack of availability in an "intermittent" fashion, environmental impacts, and the need for energy storage and conversion. Thus, improvements in energy conversion technologies will be essential to supporting the integration of renewable energy sources into a broader, more sustainable energy system.

An example of an energy conversion technology is a fuel cell which produces electrical energy from the chemical energy contained in fuels through electrochemical reactions. Fuel cells have an exceptionally high efficiency rate and their unique operating methodology makes them appealing as an alternative form of energy production. [3]

Fuel cells, as opposed to thermodynamic engines that are restricted by the Carnot efficiency limit [4] and thus dependent on combustion as an energy source, do not suffer from this limitation. The U.S Department of Energy claims that fuel cells provide significantly higher operating efficiency than traditional thermally-driven methods, as well as significantly lower amounts of harmful emissions. One of the most attractive aspects of many types of fuel cell systems is that water is their primary by-product; therefore, they have an added ecological benefit.[5]

A fuel cell consists of three primary parts: an anode, a cathode, and an electrolyte. The electrochemical reactions that occur at the interfaces of the electrodes and the electrolyte determine how well the fuel cell can perform and are also dependent on the chemical composition and physical characteristics of each of the electrodes and electrolytes used in the design of the fuel cell. All fuel cells have been considered for use in numerous applications, such as portable and stationary electricity generation, portable electronic devices, vehicular applications, and many others due to their modular design, high efficiency and low environmental impact.

1.2 Oxygen Reduction Reaction in Fuel Cells.

The electrocatalytic properties of the electrode-electrolyte interfaces are the key to how well fuel cells work. The fuel cell’s overall efficiency and output are in large part determined by the cathodic reaction (oxygen reduction reaction) and how fast it occurs.

While the ORR has a huge impact on fuel cell performance, its sluggish reaction kinetics limit it from providing the performance capabilities for fuel cells as it should. Therefore, the energy losses and limitations in the performance of fuel cells are primarily attributable to the ORR.

The current investigation will seek to evaluate the proton exchange membrane fuel cell (PEMFC) performance given the low operational temperature (80°C), and performance characteristics (low operational temperature, low operational volume, high power density and no emission from the PEMFC (only product from the PEMFC is water)). In a PEMFC, hydrogen is oxidized at the anode (the positive electrode) and produces protons and electrons, and oxygen is reduced at the cathode (the negative electrode) and combines with the protons and electrons to produce both water and produce electricity.[6]

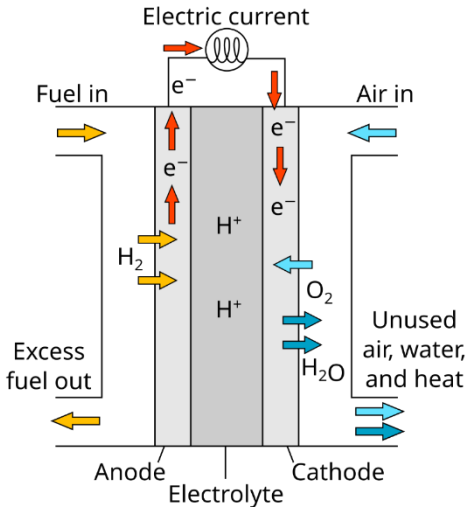

Figure 1.2 The working mechanisms of the fuel cells [7]

Under acidic conditions in a fuel cell, the ORR ideally consists of the conversion of oxygen into water through a four-electron pathway, as shown in Equation (1.1):

$$O_2 + 4H^+ + 4e^- \rightarrow 2H_2O \quad (1.1)$$

However, the ORR in acidic media may also proceed via a two-electron pathway, leading to the formation of hydrogen peroxide as an intermediate or final product, as described in Equation (1.2):

$$H_2O_2 + 2H^+ + 2e^- \rightarrow 2H_2O \quad (1.2)$$

Under alkaline conditions, the ORR follows a four-electron pathway to form hydroxide ions (OH^-), as shown in Equation (1.3):

$$O_2 + 2H_2O + 4e^- \rightarrow 4OH^- \quad (1.3)$$

Similarly, a two-electron pathway can occur in alkaline media, resulting in the formation of hydroperoxide species, as expressed in Equation (1.4):

$$HO_2^- + H_2O + 2e^- \rightarrow 3OH^- \quad (1.4)$$

The four-electron route for ORR is the most efficient and does not involve peroxide species, which would degrade over life due to the high energy charge of this route. The steps of the mechanism for ORR can be broken down into three different elementary processes: (1) oxygen binding to the electrode surface; (2) cleavage of the O-O bond; (3) transfer of electrons and protons. For these reasons, the kinetics for ORR are very complex.

Since ORR has very low reaction rates, there is a loss of voltage at the cathode called an overpotential. There are three types of overpotentials: activation, ohmic and concentration losses.

- **Activation Losses (η_{act})**

Activation losses occur due to activation energies, which are prominent for ORR. A simplified description, following a Tafel-type equation, for activation losses can be expressed by Equation (1.5):

$$\eta_{\text{act}} = \frac{RT}{\alpha n F} \ln\left(\frac{i}{i_0}\right) \qquad (1.5)$$

where i is the current density, i_0 is the exchange current density, α is the charge transfer coefficient, n is the number of transferred electrons, R is the gas constant, T is the temperature, and F is the Faraday constant.

- **Ohmic Losses (η_{ohm})**

The current flow of ions and electrons through the fuel cell's various parts, such as electrolytes, electrodes, and current collectors, causes energy loss due to their resistance. This is called Ohmic loss, which can be computed using Ohm's Law (Equation 1.6).

$$\eta_{\text{ohm}} = iR \qquad (1.6)$$

where R denotes the overall internal resistance of the system

- **Concentration Losses (η_{conc})**

Additionally, at high currents, oxygen reduction reaction velocity limitations can cause reactants to accumulate at the surface of the electrodes. Since reactant concentrations decrease near electrodes, mass transport limitations are reflected by Equation (1.7).

$$\eta_{\text{conc}} = \frac{RT}{nF} \ln\left(\frac{i_{\text{lim}}}{i_{\text{lim}} - i}\right) \qquad (1.7)$$

where i_{lim} is the limiting current density.

One way to quantify the contribution of these various overpotentials on the actual cell's voltage is shown in Equation 1.8, where the E^0 is the potential of a reversible cell.

The overall impact of the previously discussed losses to the real cell voltage can be given as:

$$E = E^0 - \eta_{act} - \eta_{ohm} - \eta_{conc} \quad (1.8)$$

The electric potential of a fuel cell is determined by several overpotentials associated with the electrochemical reactions occurring at the electrodes. Substantial work is being done to enhance the efficiency of electrocatalysts used in fuel cells.

The kinetic and transport limitations mentioned above result in ongoing research to develop efficient electrocatalysts that can improve the ORR kinetics and, therefore, increase the overall efficiency of fuel cells, lower energy losses, and facilitate the application of fuel cells more widely in practice.

1.3 Catalysts for ORR: From Platinum to Fe-N-C Materials

Over the past decade, catalysts for the oxygen reduction reaction (ORR) have shifted away from platinum (Pt) and toward the use of more plentiful transition metals (including steel/carbon) as one of their sources due to the cost efficiency/stability characteristics for this type of catalysis compared to Pt. An electrocatalyst is necessary in order to generate a sufficient performance from a fuel cell due to the slow kinetics associated with ORR [8]; otherwise, when an electrocatalyst is not used, the rate of the ORR is very low and energy is lost at the cathode. As a result, developing high-efficiency ORR electrocatalysts is critical to improving existing fuel cells and creating new fuel cell systems. To date, Pt has been the best-known electrocatalyst used for ORR because it effectively catalyzes the ORR and optimally catalyzes it in both alkaline and acidic conditions, as Pt directly catalyzes the four-electron reduction of O_2. [9]

Furthermore, Pt is capable of achieving optimal electrochemical activity in both acidic and alkaline mediums. However, Pt is limited or very expensive to utilize within a commercial context for many reasons [10]. Among the challenges of working with Pt are high raw material costs, low raw material supply, and susceptibility to degradation during use. More specifically, under certain conditions, platinum may dissolve or agglomerate during usage. As such, there are a sizable contingent of researchers focused on developing new types of catalysts made from non-precious metals that are widely available on earth; for example, catalysts composed of metal-nitrogen-carbon (M-N-C) compounds. M-N-C type catalysts have been identified as providing a tremendous lower-cost path while possessing catalytic activity equivalent to that of Pt for the ORR. [11]

A large portion of the research on the use of M-NC catalysts for the ORR has concentrated on alkaline electrochemical environments. M-NC catalysts are generally formed from metal atoms that are attached to nitrogen atoms in a carbon support or

structure. The assembly of both metal and nitrogen as functional groups in carbon appears to play a key role in assisting the adsorption of oxygen onto the ORR catalyst and facilitating the transport of electrons through the ORR catalyst.[12]

There are several different types of M-N-C catalysts, and iron-based M-N-C catalysts appear to be some of the best materials for ORR.[13] Iron is a low-cost, environmentally-friendly alternative to other metal materials, especially at low electrochemical potentials where it outperforms noble metals. The use of iron and nitrogen-containing M-N-C catalysts have also been shown to possess high catalytic activity, especially in alkaline electrochemical environments, and to be steadily increasing in catalytic activity in acidic environments as well.[14] However, there are several limitations to using iron and nitrogen-containing M-N-C catalysts including low concentration of active sites, low conductivity, and low stability.

1.4 Fe-N-C Catalysts: Structure, Performance, and Challenges

The Fe-N-C family of catalysts is classified as one of the prospective non-precious metal materials due to the reasonably low price and abundance of both iron and carbon. The Fe-N-C based materials are the best overall combination of any of the classes of catalysts for Oxygen Reduction Reactions[15]. The two main properties that influence ORR activity are the structure and nature of the active sites, as well as the arrangement of the Fe, N, and C chemically bonded together; i.e., Fe, N, C arrangements within a carbon structure. Although there have been significant advancements made in the development of Fe-N-C based catalysts, there are still several challenges to be addressed before these catalysts can be used at their full potential in fuel cells.

1.4.1 Active sites and catalyst structure

It is widely accepted that the catalytic activity of Fe-N-C based catalysts is due mainly to the Fe-N_x sites in the catalyst, [Fe-N_x] that are distributed within a conductive carbon material; the majority of overall ORR activity is likely due to the presence of the Fe-N_x sites. The Fe-N_x sites are thought to have the greatest catalytic potential to produce ORR products by means of the complete four-electron transfer reaction pathway.[16] While the Fe-N_x sites have the highest activity of ORR, studies have also shown that N-doped carbon structures contribute to improved ORR activity, including those structures that do not contain metal coordination with nitrogen, through changes in the electronic structure of carbon that promote the stronger adsorption of oxygen to the carbon material.[17]

Fe-N-C catalysts rely on the synergistic interaction between the Fe-N_x active sites and the surrounding carbon support. Although the carbon matrix does not act as the primary catalyst, its elemental and structural characteristics play important roles in defining the ability of the Fe-N_x active sites to be accessed, used, and stabilized.[18] The Impacted

porosity was a result of the development of porous carbon structure for enhancing reactant/product transport, while high electrical conductivity of carbon allowed for better rate of electron transfer during electrochemical reaction. In addition to these properties, nitrogen added to the carbon matrix can stabilize Fe species as well as generate defect sites that can provide very active sites to improve catalysis. Hence, the synergistic relationship between Fe species, N functionalities and the carbon matrix is critical to achieving superior activity for the ORR reaction. [19]

1.4.2 Main challenges: activity, conductivity, and durability

Fe-N-C catalysts are potential substitutes for costly metals that can perform the oxygen reduction reaction. While these materials are promising candidates for use as oxygen reduction catalysts, their use is still limited in practical applications. One problem is that the density of active Fe-N_x sites is low, and the number of active Fe-N_x sites available to the reaction is also low. As a result, the maximum achievable ORR activity of Fe-N-C catalysts is significantly less than the Pt-based catalysts. Therefore, it has become an important priority to enhance the number and accessibility of active Fe-N_x sites and to improve their durability. [20]

The conductivity of carbon has an effect on the performance of Fe-N-C catalysts, and consequently on the speed at which electrons will transfer through the catalyst layer during ORR. Research has shown that the addition of functionalized carbon based materials, such as carbon nanotubes, can be extremely beneficial for enhancing electron transfer and ORR activity due in part to increased graphitization and conductivity throughout the catalyst matrix. [21]

The main issue related with Fe-N-C catalysts (especially in the acidic conditions found in proton exchange membrane fuel cells) is durability. Even though Fe-N-C materials have shown considerable activity at the ORR, they have been found to be less durable than platinum based catalysts when operating continuously because of the instability associated with the active sites that contain Fe-N_x and degradation of the carbon framework. As a result, continued loss of catalytic activity will substantially limit the viability of using Fe-N-C catalysts for practical application, and therefore continued efforts are needed to develop catalysts with high long-term durability while retaining high ORR response. [22], [23], [24]

1.4.3 Strategy for Fe-N-C synthesis: the hard template method

Catalyst development is influenced by the way the Fe-N-C catalyst is produced. The synthesis of porous carbons with controlled particle shape and high surface area occurs primarily via the hard-template method which employs the use of a solid template (SBA-15) to produce a porous carbon with predictable structure. The template helps the precursors form proper carbon structures while allowing for control of the size, shape, and distribution of the pores in the porous carbon's structure.[25]

By using a hard template, a continuous interconnected mesopore structure can be generated, which results in improved mass transport and the addition of significant numbers of active sites for the electrolyte. The ability to achieve the aforementioned type of structural control enhances the transport of oxygen and reaction intermediates through the use of Fe-N-C catalysts, as well as enabling Fe-N-C catalysts to maintain their high electrical conductivity. Therefore, the use of the hard-template method will improve both the structural characteristics and electrochemical activity of the Fe-N-C electrocatalysts.[26]

1.5 Role of dopants to boost ORR performance in M-N-C electrocatalysts

Although Fe-N-C electrocatalysts show promise for high levels of catalytic activity towards the oxygen reduction reaction, this performance is highly influenced by the electronic structure surrounding the active site as well as the physical and chemical nature of the carbon matrix. The incorporation of dopants in the cathodic material becomes a means to further increase the ORR activity of the material. The inclusion of dopants can modify the local electronic environment, create additional structural defects, and provide better charge transfer characteristics in the electrocatalyst material, resulting in higher stability and activity.[27]

Among various heteroatoms, boron and sulfur have received particular attention due to their ability to tailor the electronic structure of M-N-C catalysts and influence the coordination environment of metal-nitrogen active sites. For this reason, boron and sulfur-doped Fe-N-C catalysts are of significant interest for improving ORR performance.[28,29]

1.5.1 Effect of boron doping on Fe-N-C catalysts

Extensive research has shown that the electronic structure of carbon-based materials can be modified through doping with boron to produce electrocatalysts. Boron has a lower electron density than carbon, so the incorporation of boron atoms for some of the carbon atoms produces positively charged carbon sites on the carbon lattice surface. When oxygen binds to these positively charged carbon sites, the electronic change resulting from the binding of negatively charged oxygen molecules promotes an increase in the number of oxygen molecules that will bond to the active sites (positively charged carbon sites) of the catalyst, as well as an increase in the rate of the oxygen reduction reaction occurring at these active sites. [30,31]

Furthermore, the introduction of boron into an Fe-N-C catalyst will modify the local coordination environment around each active Fe-Nx center. This will create defects in the coordination environment of the active sites, which will therefore result in modifications of the local electron density distribution at these active sites.

Consequently, the Fe-Nx active sites will have increased intrinsic activity due to the increased accessibility of these Fe-Nx sites and the acquisition of increased intrinsic activity at the active sites. The incorporation of boron into the carbon matrix will improve the overall electrical conductivity and structural integrity of the carbon support material and will be key contributing factors for the development of conductive and efficient electron transfer during electrochemical reactions [32]. Boron-doping in the Fe-N-C catalysts results in the redistribution of electron density in the Fe-N-C catalyst causing changes to the coordination environment of the Fe-N_x active site and improves the adsorption of the oxygen, involves an increase in electrical conductivity of the catalyst, and an increase in overall ORR activity of the catalyst vs undoped Fe-N-C catalysts. Therefore, it can be assumed that Fe-N-C catalysts with boron-dopants will exhibit better ORR performance than those without boron-dopants.[33, 34]

1.5.2 Effect of sulfur doping on Fe-N-C catalysts

By producing sulfur doping in carbon supports, the incorporation of sulfur: carbon has resulted in disruptions and defects formation in the structure of the catalysts (Fe-N-C), leading to greater oxygen absorption and electrochemically active materials (ORR). The inclusion of sulfur into the carbon framework has additionally changed the electronic structure and local coordination environments of the active sites on the iron-carbon-nitrogen catalysts (Fe-N_x), thus providing more active and durable catalytic materials. [35]

The addition of sulfur to carbon will develop a unique electronic structure and will accomplish this by transferring charge from the carbon to the iron atom, creating a unique electronic structure for the active site. Developing an alternative electronic structure for the catalyst increases the active site coordination around the iron atom. Consequently, the result of the new electronic structures is improved intrinsic catalytic activity of the iron-nitrogen catalysts during the oxygen-reduction reaction. In addition to producing an alternative electronic structure for the iron-nitrogen catalyst, there are also unique attributes of sulfur-containing functional groups; as an example, they provide greater affinity for hydrophilicity, which will improve the ability of the electrolyte solution to penetrate/modify the surfaces of carbon and improve the rate at which reactants and oxygen are transported to the active sites. Increased hydrophilicity also contributes to increased surface area available for the active sites, thus providing increased mass transport and improved overall electrochemical catalytic activity during the oxygen-reduction reaction compared to sulfur-free catalysts.[36, 37]

1.6 Goal and outline of the thesis

The objective of this study is to evaluate the impact of heteroatom addition to Fe-N-C electrochemical catalysts, through both electrochemical measurement and catalyst performance. Fe-N-C electrochemical catalysts are an economical alternative to

precious metal catalysts for oxygen reduction reaction (ORR) application and will be used in conjunction with electronic conductive carbon substrates. The study will analyze the effect of incorporating both boron and sulfur heteroatom doping to Fe-N-C catalysts via hard templating on the ORR performance of the catalyst by utilizing the electrochemical characteristics of the Fe-N-C catalyst as an analytical method. In short, the study seeks to determine the effect of boron and sulfur doping onto Fe-N-C catalysts on electrocatalytic activity and kinetics for ORR via systematic experimental studies.

The energy challenges that our world is dealing with today will be discussed in Chapter 1 and how fuel cells can provide a solution for converting energy in an efficient manner. There will be some background information on the oxygen reduction reaction; however, the focus will be on electrocatalysts as they relate to ORR. This chapter will specifically focus on the Fe-N-C electrocatalyst system, examining the structural and performance parameters of this system, as well as various every day challenges associated with using this system, as well as multiple possible ways to improve ORR by doping heteroatoms.

Chapter 2 will be dedicated to providing information regarding materials, methods of synthesis, and experimental methods used throughout this study. Details regarding how the hard template was created and what methods/steps were taken to create the Fe-N-C based catalysts and how boron and sulfur were incorporated into the catalysts will be provided in this chapter. Ways that the electrodes were fabricated will also be included, as will providing the steps for using rotating disk electrode (RDE) or rotating ring-disk electrode (RRDE) techniques for evaluating ORR performance in terms of activity, selectivity, and stability. electrodes/catalyst materials will be described, including scanning electron microscopy (SEM) and energy-dispersive X-ray spectroscopy (EDX) for analyzing morphology and elemental composition.

Chapter 3 examines the characterization via physicochemical means of the as-prepared boron and sulfur-doped Fe-N-C-based catalysts that were created via hard-templating. The effects of heteroatoms and hard templating on the structure (i.e., composition and morphology) of the catalysts were assessed using energy-dispersive X-ray Spectroscopy (EDX) and Scanning Electron Microscopy (SEM).

Chapter 4 provides details and discussion regarding the results of the electrochemical testing of the prepared catalysts, with a focus on their electrochemical performance and structural characteristics.

In summary, Chapter 5 presents a summary of the major findings of this research and provides recommendations for additional future studies and/or directions.

CHAPTER 2

2. MATERIALS AND METHODS

2.1 Materials and Chemicals

The methods of synthesizing the catalysts analysed are documented in this segment, including a description of the various analytical tools used to assess the extent to which the synthesised samples possess particular chemical, physical, and electrochemical characteristics.

All the chemicals used during this project were of analytical grade, and none were purified before being used in synthesis or as characterisation standards. All work was performed under controlled conditions to provide the necessary reproducibility and consistency of the synthesised catalysts and measurements made for each experiment.

The materials and chemicals provided in this section of the report were used for all the synthesis and characterisation proceedings covered in subsequent sections. For a more detail of the specific synthesis and characterisation methods employed, please refer to the specific references within this chapter.

2.1.1 Chemicals and precursors used for catalyst synthesis

Hexagonally ordered mesoporous silica SBA-15 was synthesized and used as a hard template for the preparation of Fe-N-C-based catalysts. Pluronic P123 (poly(ethylene glycol)-block-poly(propylene glycol)-block-poly(ethylene glycol), average Mn ≈ 5800) was used as the structure-directing agent, and tetraethyl orthosilicate (TEOS, 98 wt%, Sigma-Aldrich) served as the silica precursor. Hydrochloric acid (HCl, 37 wt%) and ultrapure water (18.2 $M\,\Omega$ resistivity) were used during template synthesis.

For Fe-N-C catalyst preparation, iron(III) nitrate nonahydrate ($Fe(NO_3)_3 \cdot 9H_2O$, >98%) was used as the iron precursor and 1,10-phenanthroline (anhydrous, Sigma-Aldrich) as the nitrogen-containing ligand and carbon precursor. Ethanol (≥99.8%, Sigma-Aldrich) and deionized water were used as solvents during the impregnation process.

The silica template was removed using sodium hydroxide solution (NaOH, 2M), followed by hydrochloric acid treatment (HCl, 37 wt%) to eliminate residual metallic species. All samples were pyrolyzed under a nitrogen atmosphere (high-purity N_2).[38]

For boron-doped catalysts (Fe-N-B-C), boric acid (H_3BO_3, ≥99.5%) was introduced during the impregnation step in different amounts. For sulfur-doped catalysts (Fe-N-S-C), thiourea (CH_4N_2S, ≥99%) was used as the sulfur precursor. Apart from the addition of these heteroatom precursors, the synthesis protocol remained identical to that of the undoped Fe-N-C catalyst.

2.1.2 Gases and electrolytes for electrochemical measurements

The electrochemical measurements were conducted using high-purity gases and aqueous electrolyte solutions. The supplier supplied nitrogen (N_2) gas for purging the electrolyte solutions and to do background measurements of electrochemical properties under inert conditions. The supplier supplied O_2 gas prior to ORR measurements in the electrolyte in order to ensure saturation of the electrolyte with O_2.

Characterizations through electrochemical measurements were made in acidic and alkaline solutions. The acidic electrolyte was 0.1M Hydrogen Perchloric Acid ($HClO_4$). The alkaline solution used was 0.1M Potassium Hydroxide (KOH). Deionized water was used to prepare each one of the sources of the electrodes electrochemically prior to performing their electrochemical measurements.

For the preparation of 0.1 M $HClO_4$, a 500 mL volumetric flask was used. A volume of 4.3 mL of concentrated perchloric acid ($HClO_4$) was carefully measured and diluted with deionized water. Initially, a portion of deionized water was added to the flask, followed by the slow addition of concentrated acid with gentle mixing to ensure complete homogenization. The solution was then diluted to the final volume of 500 mL with deionized water.

In the same way, to prepare a 0.1 M KOH (500 mL), 2.8 g of KOH pellets were dissolved in deionized water using the same dilution procedure as above. The pellets were completely dissolved before adjusting to 500 mL.

All of the electrolyte solutions were purged with the appropriate gas prior to performing the corresponding electrochemical tests, thereby ensuring that the testing was performed under repeatable and consistent conditions.

2.2 Synthesis of the Hard Template (SBA-15)

SBA-15 is a mesoporous silica, made by soft templating. In making SBA-15, a triblock copolymer is a structure directing agent and tetraethylorthosilicate (TEOS) serves as a silica precursor in an acid solution. This process occurs under controlled temperature and stirring conditions to create a two dimensional (2D) hexagonal pore structure with high surface area and ordered structure and multiwall pores.[39] The SBA-15 was then used to create an Fe-N-C type catalyst using it as a hard template.

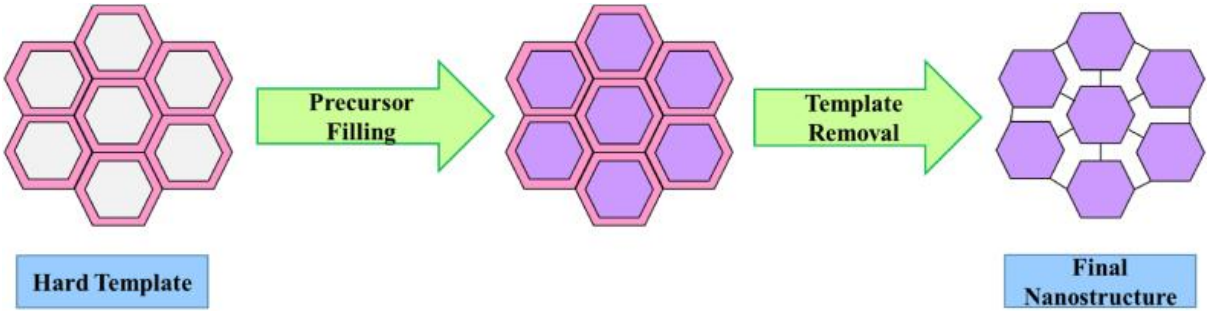

Figure 2-1 Schematic illustration of the main mechanism of the hard-template method [40]

2.2.1 Preparation of SBA-15

The synthesis was carried out in a 1L reactor placed in an oil bath maintained at 40 °C. An acidic aqueous solution was first prepared by mixing 340 mL of deionized water with 48.8 mL of hydrochloric acid under continuous stirring until complete homogenization was achieved. Once thermal equilibrium was reached, 10 g of Pluronic P123 were added to the solution. The mixture was stirred at 40 °C for 5-6 hours, allowing complete dissolution of the polymer and the formation of micellar aggregates that define the mesostructure of the template.

Subsequently, 24 mL of tetraethyl orthosilicate (TEOS) were introduced into the reaction mixture. The system was maintained under stirring at 40 °C for 20 hours, during which the silica precursor underwent hydrolysis and condensation around the polymeric micelles, leading to the formation of an ordered silica-polymer composite.

The resulting suspension was then subjected to hydrothermal aging at 100°C for 24 hours in an autoclave, a treatment that promotes further silica condensation and improves the structural ordering of the mesoporous framework. After aging, the reactor was allowed to cool naturally to room temperature before opening. The solid product was homogenized by stirring, recovered by vacuum filtration, and thoroughly washed several times with deionized water to remove residual acid and soluble by-products.

The collected solid was dried overnight at room temperature and finally calcined in air at 550°C, using a heating rate of 2 °C min^{-1} and a dwell time of 10 hours, to remove the organic template and obtain the ordered mesoporous SBA-15 silica used as hard template in the subsequent Fe-N-C synthesis.

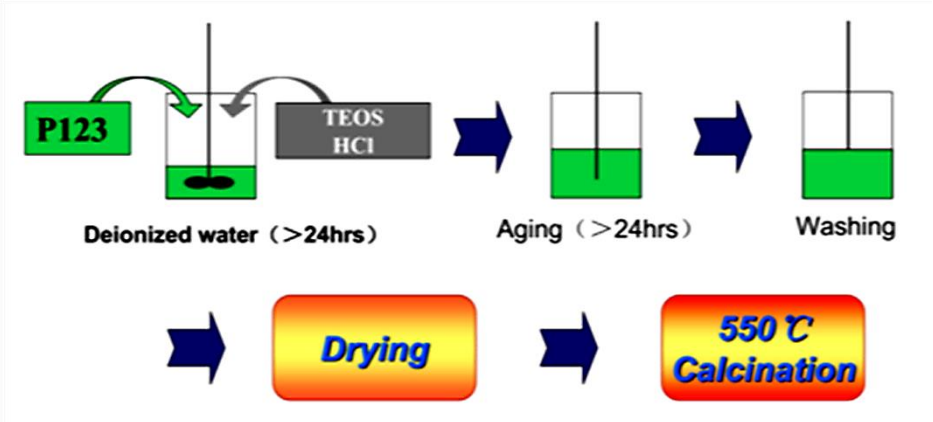

Figure 2-1 Schematic representation of the synthesis and preparation method of SBA-15. [41]

2.3 Synthesis of Fe-N-C Based Catalysts

Fe-N-C-based catalysts were synthesized using SBA-15 as a hard template. The synthesis procedure involved the impregnation of carbon, nitrogen, and iron precursors into the mesoporous silica framework, followed by two pyrolysis steps, the first after the precursors mix step and the second after the washing step. Variations of the same procedure were applied to obtain boron- and sulfur-doped catalysts.

2.3.1 Synthesis of Fe-N-C catalys

The Fe-N-C catalyst was synthesized using SBA-15 as a hard template. In a typical synthesis, 500 mg of SBA-15 was dispersed in a mixed solvent composed of 10 mL deionized water and 10 mL ethanol. The solvent mixture was placed under magnetic stirring, and SBA-15 was added gradually until a homogeneous suspension was obtained.

In parallel, an oil bath was prepared by heating a container filled with oil on a hot plate to 75°C. The temperature was allowed to stabilize before further use. A second precursor solution was then prepared by mixing 5 mL deionized water and 5 mL ethanol under magnetic stirring. After obtaining a homogeneous solvent mixture, 400 mg of iron(III) nitrate nonahydrate ($Fe(NO_3)_3 \cdot 9H_2O$) and 492 mg of 1,10-phenanthroline were added simultaneously. The mixture was stirred until complete dissolution of the precursors and formation of a homogeneous solution.

The SBA-15 suspension was subsequently added to the iron-nitrogen precursor solution under continuous stirring to ensure uniform impregnation of the silica template. The resulting mixture was transferred to the preheated oil bath and maintained at 75°C for 24 hours. This step allowed effective infiltration of the precursors into the mesoporous structure of SBA-15. The container was labeled according to the sample composition and treatment duration.

After completion of the aging step and subsequent drying, the resulting solid precursor was subjected to a first pyrolysis treatment in a tubular oven under a continuous nitrogen atmosphere. The temperature was increased to 900 °C at a heating rate of 5 °C min^{-1} and maintained at this temperature for 3 hours. This thermal treatment was carried out to promote carbonization and to stabilize the Fe-phenanthroline complexes within the SBA-15 template structure.

Following the first pyrolysis, the silica template was subsequently removed by chemical etching. The carbonized material was prepared by dissolving 12.8 g of NaOH in a mixed solvent containing 80 mL of deionized water and 80 mL of ethanol under magnetic stirring at room temperature until complete dissolution was achieved.. The suspension was then centrifuged and washed three times with deionized water until a neutral pH was reached. Afterwards, the solid was treated with an HCl solution (prepared from 37 wt% HCl) for 3 h to remove residual metal species. The mixture was again centrifuged

and washed twice with deionized water and once with ethanol until neutral pH (pH > 4) was achieved, and finally dried overnight at 50 °C.

Finally, the dried sample was subjected to a second pyrolysis under nitrogen using the same conditions as the first treatment (900 °C, 5 °C min^{-1}, 3 hours) to further graphitize the carbon framework and enhance its conductivity and stability.

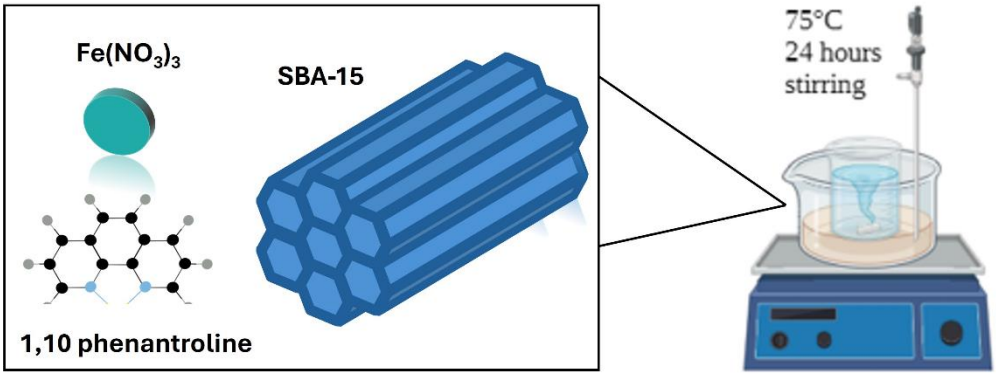

Figure2-2 Precursor mixing and solubilization for Fe–N–C catalyst synthesis.(42)

2.3.2 Boron-doped Fe-N-C catalysts

Boron-doped Fe-N-C catalysts (Fe-N-B-C) were synthesized following the same procedure used for the undoped Fe-N-C catalyst, with the use of boric acid (H_3BO_3) as the boron source during the precursor preparation step. After the addition of iron(III) nitrate nonahydrate and 1,10-phenanthroline to the water-ethanol mixture, boric acid was added in amounts corresponding to 25% ($FeN_{0.75}B_{0.25}C$), 50% ($FeN_{0.5}B_{0.5}C$), and 75% ($FeN_{0.25}B_{0.75}C$) relative to the nitrogen content.

Specifically, 111 mg of boric acid was used for the 25% B-doped sample, while 338 mg and 1012 mg were added for the 50% and 75% B-doped samples, respectively. Upon the addition of the boron precursor, the SBA-15 suspension was added with constant stirring. The remaining synthesis steps, including thermal treatment at 75 °C for 24 hours, were identical to those employed for the Fe-N-C catalyst, resulting in a series of Fe-N-B-C materials with increasing boron content.

The goal of adding boron was to alter the electronic structure of the carbon matrix, create more catalytically active sites, and improve conductivity and stability, all of which would lead to improved ORR activity compared to nonboron-doped Fe-N-C catalysts.

After drying in an oil bath, all of the proceeding treatments (i.e., pyrolysis, removal of the silica template, acid leaching, washing, drying, and second pyrolysis) for the boron substituted materials were conducted exactly as with the nonboron-doped Fe-N-C catalysts.

2.3.3 Sulfur-doped Fe-N-C catalysts

Sulfur-doped Fe-N-C catalysts (Fe-N-S-C) were synthesized using the same synthesis protocol adopted for Fe-N-C, replacing boric acid with thiourea as the sulfur source. Thiourea was added after the incorporation of iron(III) nitrate nonahydrate and 1,10-phenanthroline into the water-ethanol solvent mixture, using amounts corresponding to 25% ($FeN_{0.75}S_{0.25}C$), 50% ($FeN_{0.5}S_{0.5}C$), and 75% ($FeN_{0.25}S_{0.75}C$) relative to the nitrogen content.

Specifically, 70 mg, 208 mg, and 780 mg of thiourea were employed for the 25%, 50%, and 75% S-doped samples, respectively. After complete dissolution of the precursors, the SBA-15 suspension was added and the mixture was processed following the same conditions used for the Fe-N-C and Fe-N-B-C syntheses, including the thermal treatment at 75 °C for 24 hours.

The introduction of sulfur heteroatoms was aimed at enhancing the density of active sites, improving charge transport properties, increasing catalyst stability, and ultimately achieving enhanced ORR performance relative to conventional Fe-N-C catalysts.

The procedures for pyrolysis and removal of the silica template, acid leaching and washing, drying, and the second pyrolysis were the same as those used with the Fe-N-C catalyst.

2.4 Electrode Preparation

The preparation of working electrodes is the critical step to allow for the electrochemical evaluation of synthesized iron-nitrogen-carbon (Fe-N-C) based catalysts. To provide reproducible and trustworthy electrochemical measurements, a consistent process was utilized to formulate the catalyst ink and deposit it on glassy carbon electrode. This process worked to ensure (i) homogenous dispersion of the catalyst, (ii) durability of the electrode film, and (iii) control of the amount of catalyst loaded onto the electrode via electrochemical techniques.

2.4.1 Catalyst ink preparation

Catalyst inks were prepared by dispersing 2 mg of Fe-N-C-based catalyst powder in 400 μL of isopropanol (IPA, ≥99.7%) and 10 μL of Nafion solution (5 wt%). Nafion was used as a proton-conducting ionomer and binder to ensure proper adhesion of the catalyst layer to the glassy carbon electrode and to provide ionic conductivity within the catalyst film.

The Nafion content was selected to obtain an ionomer-to-carbon (I/C) ratio of 0.2 for the Fe-N-C catalysts. This ratio was chosen as a compromise between ensuring

sufficient proton transport and maintaining accessibility of the active Fe-N_x sites. Excessive ionomer content can block catalytic sites and hinder oxygen diffusion, whereas insufficient ionomer may result in poor mechanical stability and non-uniform films.

For comparison, a reference ink was prepared using commercial 40 wt% Pt/C. In this case, 2 mg of Pt/C were dispersed in 2 mL of isopropanol and 5.5 µL of Nafion solution (5 wt%). The Pt/C ink composition was adjusted to ensure appropriate film adhesion and uniformity while maintaining consistent electrode preparation conditions for reliable benchmarking against the synthesized catalysts.

All suspensions were ultrasonicated for 15 minutes to ensure homogeneous dispersion and minimize particle agglomeration. The inks were used immediately after sonication to prevent sedimentation and to ensure reproducible catalyst loading during electrode preparation.

2.4.2 Drop-casting on glassy carbon

The prepared catalyst ink was subsequently deposited onto the disk electrode using a drop-casting technique. Prior to deposition, the glassy carbon electrode surface was cleaned and prepared as described previously to ensure proper adhesion of the catalyst layer.

A fixed volume of 10.3 µL of the catalyst ink was carefully drop-cast onto the glassy carbon disk electrode. This volume corresponded to a target catalyst loading of 0.4 mg cm^{-2}, ensuring consistent and reproducible electrode preparation across all measurements. Following deposition, the electrode was left to dry completely under ambient conditions, allowing for gradual solvent evaporation and the formation of a uniform and mechanically stable catalyst film.

After complete drying, the electrodes were ready for electrochemical characterization using rotating disk electrode (RDE) and rotating ring-disk electrode (RRDE) techniques.

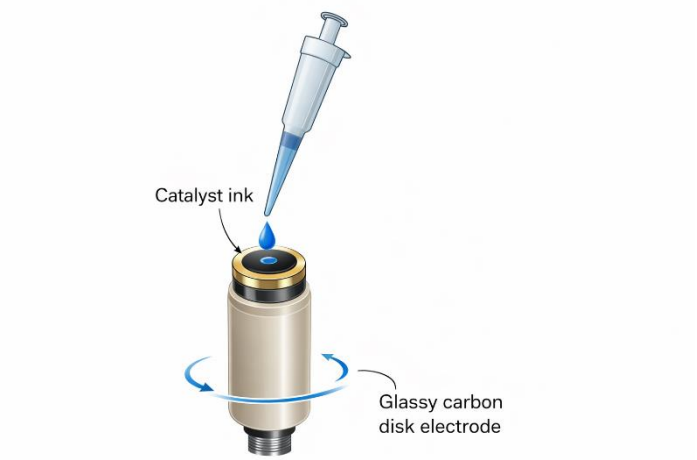

Figure2-3 Schematic illustration of catalyst ink drop-casting of catalyst ink on a glassy carbon disk electrode.

2.5 Electrochemical Characterization: RDE and RRDE

Electrochemical characterization of the synthesized catalysts was carried out using rotating disk electrode (RDE) and rotating ring-disk electrode (RRDE) techniques to evaluate their activity toward the oxygen reduction reaction. These techniques allow the investigation of reaction kinetics, mass transport effects, and reaction pathways under well-controlled hydrodynamic conditions. Measurements were performed in both acidic and alkaline environments to assess catalyst performance under different operating conditions.

2.5.1 RDE and RRDE analysis

Rotating disk electrode (RDE) and rotating ring-disk electrode (RRDE) techniques were employed to analyze the electrochemical behavior of the synthesized catalysts toward the oxygen reduction reaction. These techniques provide quantitative information on reaction kinetics, mass transport effects, and reaction pathways under well-defined hydrodynamic conditions.

In RDE measurements, the rotation of the disk electrode induces a controlled convective flow of electrolyte toward the electrode surface, ensuring a constant diffusion layer thickness. Under diffusion-limited conditions, the limiting current density (i_{lim}) depends on the rotation speed of the electrode and can be described by the Levich equation:

$$i_{lim} = 0.62\, n\, FAD_0^{\frac{2}{3}} v^{\frac{1}{6}} \omega^{\frac{1}{2}} C \quad (2.1)$$

where i_{lim} is the diffusion-limited current density, n is the number of electrons transferred per oxygen molecule, F is the Faraday constant (96,485 C/mol), A is the area of electrode (cm^2), D is the diffusion coefficient of oxygen in the electrolyte (cm^2/s), v is the kinematic viscosity of the electrolyte (cm^2/s), C is the bulk concentration of dissolved oxygen (mol/cm^3), and ω is the angular rotation speed of the electrode (rad/s). Typical parameter values used for RDE analysis in 0.1 M KOH and 0.1 M $HClO_4$ are summarized in Tables 2.1 [43] and 2.2 [44].

D [cm^2/s]	$1.9e^{-5}$
ν [cm^2/s]	$9e^{-3}$
C [mol/cm^3]	$1.26e^{-3}$

Table 2.1 Levich equation parameters (0.1M KOH)

D [cm^2/s]	$1.93e^{-5}$
ν [cm^2/s]	$1.01e^{-2}$
C [mol/cm^3]	$1.26e^{-3}$

Table 2.2 Levich equation parameters (0.1M $HClO_4$)

Koutecký-Levich analysis was performed using LSV data acquired at different rotation speeds (400-2500 RPM) to separate kinetic and diffusion-controlled contributions to the measured current and to further assess ORR kinetics.

When both kinetic and diffusion contributions affect the measured current, the system can be described by the Koutecký-Levich (K-L) equation:

$$\frac{1}{i} = \frac{1}{i_k} + \frac{1}{i_{lim}} \qquad (2.2)$$

where i is the measured current density, i_k is the kinetically controlled current density, and i_{lim} is the diffusion-limited current density described by Eq. (2.1).

Koutecký-Levich analysis was used to separate kinetic and mass-transport contributions. The slope of the linear K-L plot is given by:

$$\frac{1}{i_{\text{lim}}} = \frac{1}{0.62\, nFAD_0^{2/3} \nu^{1/6} \omega^{1/2} C} \qquad (2.3)$$

The slope was used to determine the apparent number of electrons transferred (n) during ORR and to assess the dominant reaction pathway.

During RRDE experiments, both disk and ring currents were recorded simultaneously. The collected disk and ring currents were used to calculate the hydrogen peroxide (H_2O_2) yield and the number of electrons transferred during the ORR process.

The apparent electron transfer number was calculated using:

$$n = 4 \left(\frac{I_d}{I_d + I_r / N} \right) \qquad (2.4)$$

where I_d and I_r represent the disk and ring currents, respectively, and N is the collection efficiency factor of the RRDE system. The collection efficiency has been experimentally derived from a well defined redox system and can be expressed as:

$$N = \frac{I_R}{I_D} \qquad (2.5)$$

The percentage of hydrogen peroxide produced during ORR was calculated according to:

$$\%\, H_2O_2 = 200 \times \frac{I_r}{N \times (I_d + I_r/N)} \qquad (2.6)$$

These equations were used to evaluate ORR kinetics, electron transfer number, and peroxide formation based on RDE and RRDE experimental data.

2.5.2 Electrochemical setup

To perform electrochemical tests on the newly developed Fe-N-C catalyst material, RRDE (rotating ring disk electrode) setups were used. Prior to performing a test, the disk electrodes (type of glassy carbon) used were polished with a polishing kit to remove any contamination and form a smooth surface. Following this, all polished electrodes were rinsed with de-ionised water and placed in the RRDE test apparatus.

In these tests, a three electrode cell was used as the electrochemical test cell, with the prepared disk electrodes (which had been catalyst coated) used as the working electrode. An Ag/AgCl reference electrode was used in the acidic 0.1 M HClO4 electrolytic test solution, while a $Hg/HgSO_4$ reference electrode was used in the alkaline 0.1 M KOH electrolytic test solution. In addition, all potential measurements were converted and reported based on the RHE (reversible hydrogen electrode). The counter electrode used in these tests was a carbon rod.

As the electrolytic test solution, both 0.1 M $HClO_4$ and 0.1 M KOH were used. Prior to each electrochemical test being performed, the electrolyte was purged with high-purity nitrogen (N_2) to ensure no dissolved oxygen was in the electrolyte, as well as to establish a stable baseline for all tests.

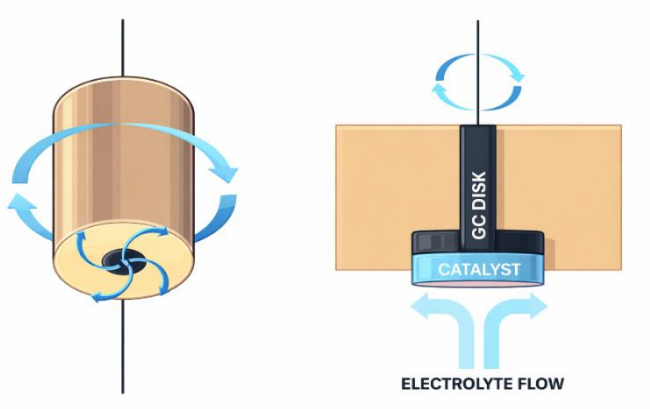

Figure 2-4 Schematic illustration of a rotating disk electrode (RDE) setup, depicting the electrolyte flow induced by electrode rotation.

2.5.3 Cyclic voltammetry and linear sweep voltammetry measurements

The electrochemical protocol began with cyclic voltammetry (CV) measurements under nitrogen-saturated conditions. An initial series of CV scans was performed at a scan rate of 500 mV s^{-1} to clean the electrode surface, remove residual contaminants, and stabilize the catalyst-electrolyte interface and electrochemical Cleaning. Subsequently, CV measurements were carried out under nitrogen at a reduced scan rate of 100 mV s^{-1}.

Following the nitrogen-based measurements, linear sweep voltammetry (LSV) scans were conducted under nitrogen at a scan rate of 10 mV s^{-1} to establish the background current. The electrolyte was then saturated with oxygen (O_2), and CV measurements were repeated at a scan rate of 100 mV s^{-1}. LSV measurements under oxygen-saturated conditions were performed at a scan rate of 10 mV s^{-1}.

To evaluate ORR kinetics and mass transport behavior, LSV measurements were conducted at rotation speeds of 400, 900, 1600 and 2500 rpm. The potential window applied ranged from 0.05 to 1.2 V vs. RHE for CV measurements and from 0 to 1.2 V vs. RHE for LSV measurements.

2.5.4 Trochemical impedance spectroscopy (EIS) measurements

Electrochemical impedance spectroscopy (EIS) measurements were performed under oxygen-saturated conditions to probe the interfacial properties of the catalyst layer during the oxygen reduction reaction. EIS analysis was used to investigate the resistive and kinetic characteristics of the electrochemical system, providing complementary information to the kinetic behavior observed in linear sweep voltammetry and RRDE measurements.

The impedance spectra were recorded by applying voltage with an amplitude of 10 mV around a fixed applied potential of 0.5 V vs. RHE with frequency range 10000-1 Hz. Measurements were carried out under a continuous O_2 flow to ensure ORR-relevant conditions. The obtained impedance data enabled the determination of ohmic resistance and charge-transfer resistance, supporting the interpretation of charge transport and interfacial processes governing ORR performance.

2.5.5 Stability tests

The electrochemical stability of the synthesized catalysts was evaluated after completion of the RDE and RRDE performance measurements. Stability tests were conducted under oxygen-saturated conditions to assess the durability of the catalysts during prolonged operation relevant to the oxygen reduction reaction.

The chronoamperometry (CA) test was performed at a fixed potential of 0.68 V RHE and a constant rotation rate of 1600 rpm and maintained continuously for a duration of 4 hours. This procedure allowed the evaluation of potential degradation effects on catalytic activity under steady-state hydrodynamic and reaction conditions.

Following stability testing, electrochemical measurements were made again to evaluate any electrochemical performance changes related to the ORR. Linear sweep voltammetry and RRDE measurements were performed at 1600 rpm under identical conditions to those that were used in measuring the LSVs and RRDEs before stability testing. Comparison of the LSV polarization curves and RRDE data before and after the stability test provided a better understanding of the changes in catalytic activity, selectivity, and reaction pathway caused by long-term electrochemical operation.

2.6 Chemical and Physical Characterization Methods

In order to characterize the structural and morphological characteristics of synthesized boron-doped and sulfur-doped catalysts based on Fe-N-C, both chemical and physical characterizations were conducted using a variety of methods to obtain complementary information, in addition to electrochemical testing, which is critical to understanding the relationship between structure and performance of Fe-N-C based catalysts.

The principal physicochemical methods used to evaluate the synthesized catalytic structures were: Energy Dispersive X-ray (EDX) spectroscopy and Scanning Electron Microcopy (SEM).

2.6.1 Energy dispersive x-ray spectroscopy

Energy dispersive x-ray spectroscopy (EDX) is an analytical approach that provides information on the elemental makeup of materials in a solid-state. This technique uses a focused beam of electrons interacting with a sample to produce X-rays back at the sample surface based on the composition of the sample. Each element found within the sample produces characteristic X-rays based on energy levels that are unique to that element; thus qualitative and semi-qualitative elemental analysis of the sample can be made [45].

EDX and SEM were used for the characterization of Fe-N-C catalysts with respect to their elemental composition and distribution of elements throughout the catalysts. The evaluation indicated that the catalysts contained carbon (C), nitrogen (N), iron (Fe) and any doped heteroatoms (e.g., boron or sulfur) that may have been added into the catalyst systems. The elemental mapping associated with EDX provided a method for evaluating elemental homogeneity across each catalyst surface for all four elements.

The dispersion of iron and heteroatoms within the catalyst are important because the arrangement of the active sites will affect both their activity and longevity. Therefore, EDX offers crucial insights regarding the elemental makeup of the catalysts that can be used in conjunction with electrochemical characterization data.

2.6.2 Scanning Electron Microscopy (SEM)

Scanning Electron Microscopy (SEM) is a very functional imaging technique that allows the investigation of the surface's morphology and the describing the microstructure of the materials. This research employed a FESEM Zeiss SUPRA 40 based Scanning Electron Microscope, to analyze the morphology of the materials produced, the texture of the material's surface, and the structural integrity of the synthesized catalysts.

Using SEM provides an in-depth and detailed qualitative basis for evaluating the particle morphology, particle size distribution, and surface characteristics of materials

being examined with Scanning Electron Microscopy (SEM). Since the catalysts were manufactured with Nitrogen-doped Carbon (Fe-N-C) based catalysts, the assessment of the effectiveness of the catalytic synthesis method is essential. Therefore, SEM has demonstrated the efficacy of using Scanning Electron Microscopy to characterize porous structures in the synthesis of the porous structure, the overall morphology of the carbon structure, and how the morphology of the catalyst would ultimately affect mass transfer to and accessibility to the catalyst during electrochemical reactions.

3. RESULTS AND DISCUSSION : Physico-Chemical characterization

3.1 Energy dispersive x-ray spectroscopy (EDX)

$FeNB_xC$ Series (Boron-Doped Catalysts)

The energy-dispersive X-ray analysis of the $FeNB_xC$ catalysts shows the presence of the major elements: carbon, nitrogen, iron, and boron. Among these elements, the major component is carbon, which is expected for Fe-N-C catalysts synthesized from the carbonization of organic precursors. The presence of nitrogen is due to the phenanthroline precursor used in the synthesis.

$FeNB_{0.25}C$	Weight%	Atomic%	$FeNB_{0.5}C$	Weight%	Atomic%	$FeNB_{0.75}C$	Weight%	Atomic%
B K	9.51	11.02	B K	13.77	19.38	B K	16.37	19.08
C K	75.32	78.53	C K	27.17	34.41	C K	61.26	64.26
N K	4.43	3.96	N K	5.04	5.48	N K	9.39	8.45
O K	6.16	4.82	O K	29.67	28.21	O K	8.00	6.30
Si K	2.89	1.29	Si K	21.89	11.86	Si K	3.51	1.58
Fe L	1.69	0.38	Fe L	2.45	0.67	Fe L	1.47	0.33
TOTALS	100		TOTALS	100		TOTALS	100	

Table 3.1 The elemental composition of the $FeNB_xC$ catalysts obtained from EDX analysis.

Boron is present in all samples, confirming the incorporation of the boron precursor. However, the amount of boron exceeds the calculated amount based on the chemical composition of the synthetic material. This discrepancy may be due to the limitations of energy-dispersive X-ray spectroscopy, which has difficulty detecting light elements, and the B peak appears at very low energy (eV) and may even coincide with the carbon peak, thus overestimating the boron concentration.

Apart from the main elements, oxygen and silicon are present. Oxygen is likely due to surface oxidation of the carbon material, whereas silicon is likely due to the incomplete removal of the silica template from the SBA-15 material.

Significant variation is observed with regard to the elemental composition of the samples. For instance, the $FeNB_{0.5}C$ sample has higher levels of oxygen and silicon, which could imply the presence of higher levels of silica, which may not have been completely removed during the etching process. This observation is in line with the morphological study, which indicated that the boron-doped samples do not perfectly mimic the ordered framework of SBA-15. It is possible that the boron precursor is located outside the pores, rather than inside, during the impregnation process.

In general, it can be concluded that EDX is an affirmation of the boron content in $FeNB_xC$; however, it is necessary to note that these results should be used with caution due to limitations in the analysis of light elements by EDX.

$FeNS_xC$ Series (Sulfur-Doped Catalysts)

It can be concluded that EDX analysis of the FeNSxC catalysts indicates the presence of the main elements present in the synthesized materials, namely carbon, nitrogen, iron, and sulfur. Carbon was found to dominate all of the samples, as expected due to the formation of a carbon-based catalyst structure. Nitrogen was also found in all of the samples, as expected due to the presence of nitrogen-containing species from the phenanthroline ligand.

$FeNS_{0.25}C$	Weight%	Atomic%	$FeNS_{0.5}C$	Weight%	Atomic%	$FeNS_{0.75}C$	Weight%	Atomic%
B K	76.63	84.86	B K	81.98	89.07	B K	73.65	84.21
C K	5.70	5.41	C K	3.11	2.89	C K	3.37	3.30
N K	7.43	6.18	N K	6.25	5.10	N K	6.63	5.69
O K	2.41	1.14	O K	2.24	1.04	O K	7.53	3.68
Si K	3.11	1.29	Si K	2.33	0.95	Si K	5.18	2.22
Fe L	4.73	1.13	Fe L	4.11	0.96	Fe L	3.64	0.90
TOTALS	100		TOTALS	100		TOTALS	100	

Table 3.2 The elemental composition of the $FeNS_xC$ catalysts obtained from EDX analysis.

According to the results, sulfur was also present in all these materials, confirming that this element was incorporated into these materials. A clear trend of composition from one material to another was observed in the $FeNS_xC$ catalyst series, i.e. from $FeNS_{0.25}C$ to $FeNS_{0.75}C$, with increasing sulfur content.

These relative iron-to-nitrogen ratios are within comparable ranges for all the samples, thus implying that the presence of sulfur does not significantly affect the formation of Fe-N_x active sites within the carbon material. There are also some minor peaks for oxygen and silicon. The presence of oxygen is due to the oxidation of the carbon structure, whereas the presence of silicon is due to the silica template from the SBA-15 template used during the synthesis. This implies that there are some residues from the template even after the removal.

As a summary, the EDX results have confirmed the successful doping of sulfur throughout the series of $FeNS_xC$ samples, as well as the presence of the expected composition trend as a result of the increased sulfur doping. Compared to the boron-doped catalysts, the sulfur-doped catalysts have more consistent elemental responses, thus implying a more successful doping effect within the templated carbon structure.

Discussion

A comparative analysis of the $FeNB_xC$ and $FeNS_xC$ catalyst series indicates the presence of differences in the dopants' incorporatioof dopants thin the Fe-N-C matrix. The presence of the dopants in the $FeNB_xC$ and $FeNS_xC$ series was verified using energy-dispersive X-ray spectroscopy, and the $FeNS_xC$ series indicates a clearer and more consistent trend in the composition, suggesting the effectiveness of the sulfur doping depends on the composition of the precursors used. The quantification of boron within the $FeNB_xC$ catalyst series was not as clear due to the low energy of the boron peak and the possibility of overlap with the carbon peak during the EDX analysis. The results suggest the effectiveness of the doping was qualitatively verified but quantitatively difficult.

3.2 Scanning Electron Microscopy (SEM)

Scanning Electron Microscopy was employed to investigate the morphology and surface characteristics of the synthesized Fe-N-C based materials. This technique provides detailed information on the microstructural features of the samples, including particle shape, aggregation behavior, and surface texture. Through SEM analysis, it is possible to evaluate the overall structural organization of the carbon framework and assess the influence of the synthesis conditions and dopant species on the resulting morphology. In particular, SEM observations allow the identification of differences in particle distribution and structural compactness between the various samples, providing important insights into the effectiveness of the templating and carbonization processes.

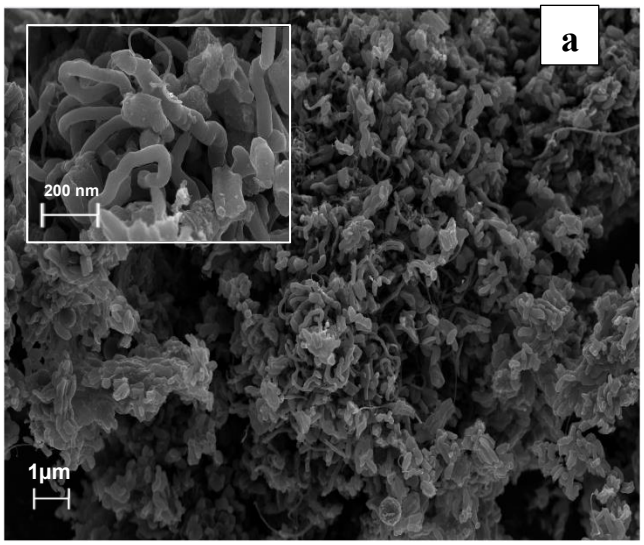

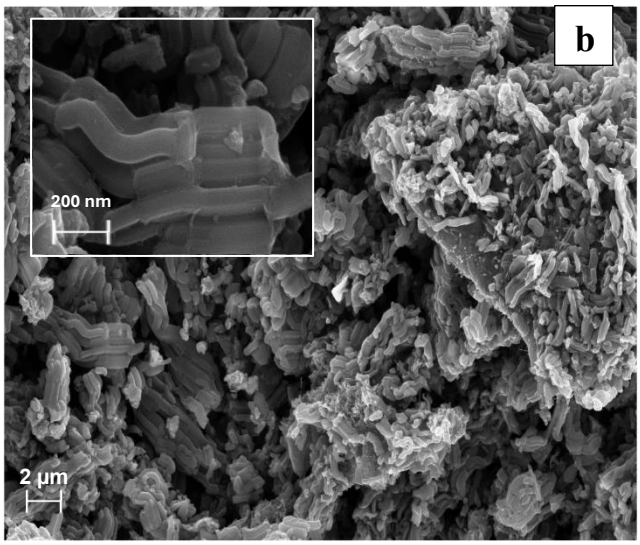

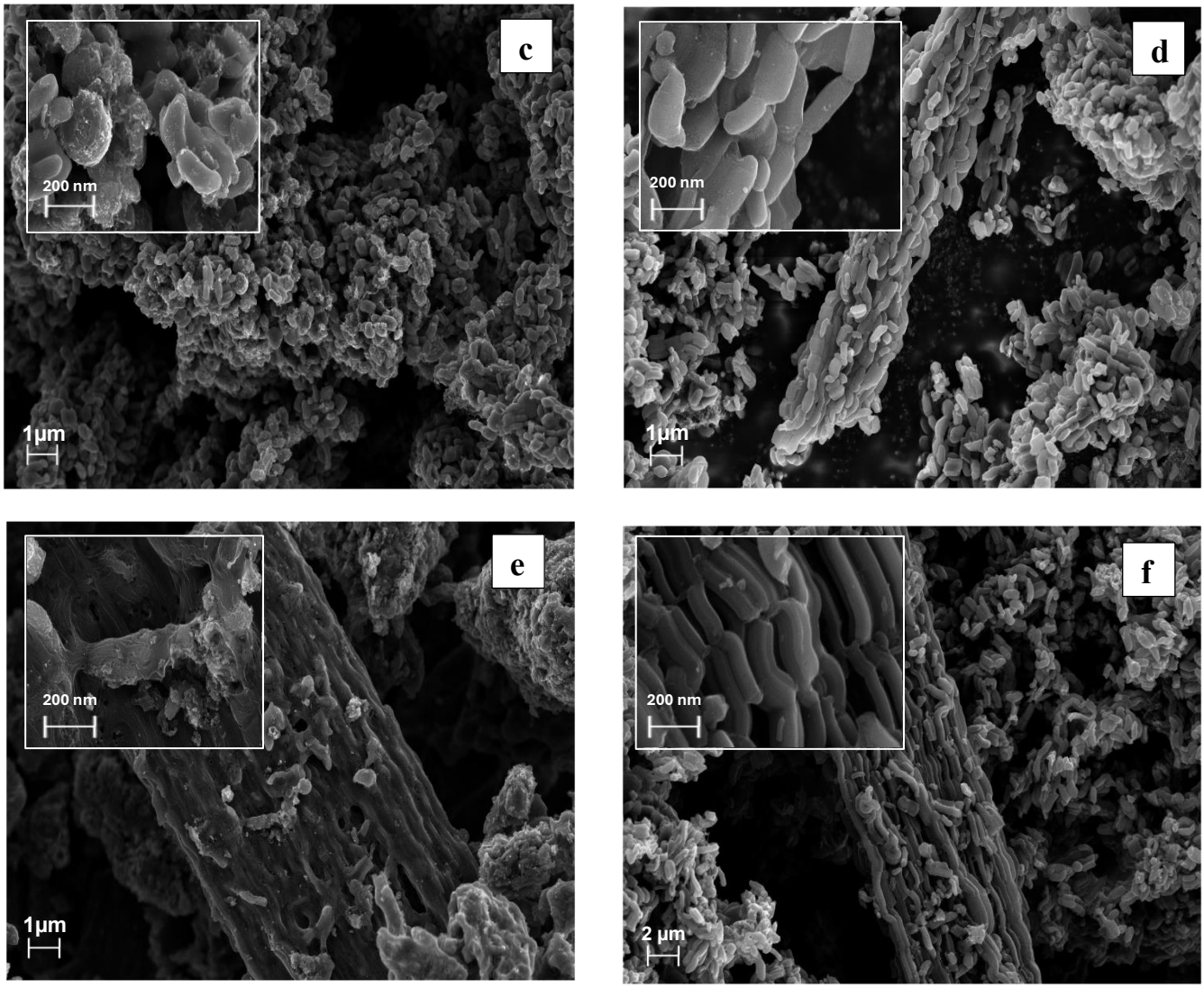

Fig. 3.1 SEM images of $FeNB_xC$ and FeN_xSC samples at different compositions: a) $FeNB_{0.25}C$, b) $FeNS_{0.25}C$, c) $FeNB_{0.5}C$, d) $FeNS_{0.5}C$, e) $FeNB_{0.75}C$, and f) $FeNS_{0.75}C$ (large images: low magnification 10k , inset images: high magnification 80k).

A comparative analysis of the SEM images reveals clear morphological differences between the $FeNB_xC$ and $FeNS_xC$ samples, indicating that the type of dopant significantly influences the structural organization of the carbon materials.

For samples prepared with minimum precursor content ($FeNB/S_{0.25}C$), both materials consist of aggregated particles of irregular morphology. However, in the case of $FeNB_{0.25}C$, these particles are arranged in compact aggregates with minimal porosity between particles. On the contrary, in the case of the $FeNS_{0.25}C$ sample, these particles are arranged in a more open manner, with aggregates that are less compact and exhibit identifiable spaces between them. Although both materials exhibit irregular surface features characteristic of nanostructured carbons, the latter appears less compact in its structure.

An analogous phenomenon is noted for the materials synthesized using intermediate precursor concentration (FeNB/$S_{0.5}$C). The $FeNB_{0.5}$C material still shows densely aggregated irregular carbon fragments, leading to the formation of a compact structure. The $FeNS_{0.5}$C material shows a less dense structure of aggregates, where the clusters are more apart from each other, indicating the presence of void spaces. This shows a difference in the morphology of the two materials. The surface roughness of the two materials is similar at the nanoscale level. The $FeNS_{0.5}$C material shows a less compact structure.

This phenomenon is noted for the materials synthesized using the highest precursor concentration (FeNB/$S_{0.75}$C). The $FeNB_{0.75}$C material shows large aggregates of irregular carbon particles, indicating a compact structure. The $FeNS_{0.75}$C material shows an open structure of loosely aggregated irregular particles. The surface roughness of the two materials is similar at the nanoscale level. The $FeNS_{0.75}$C material shows a less compact structure.

SEM results show that there is a clear distinction in the morphology of the two series of samples: whereas $FeNB_x$C materials have a clear preference for the formation of compact carbon clusters, the $FeNS_x$C samples have a more open and loosely arranged particle structure. The more open structure of the $FeNS_x$C samples suggests a better preservation of the structural features introduced by the SBA-15 template, as opposed to the $FeNB_x$C samples, which have a clear tendency to lose the templated structure and form compact clusters. This could be due to the interaction of the precursors with the silica template during impregnation, with boron species not interacting with the template from the inside but instead from the outside.

4. RESULTS AND DISCUSSION : Electrochemical Characterization

4.1 Electrochemical Characterization: Rotating (Ring) Disk Electrode

The electrochemical results obtained for the synthesized Fe-N-C-based catalysts. The focus is placed on evaluating the oxygen reduction reaction activity, kinetics, selectivity, and stability of the materials, and on understanding how heteroatom doping with boron and sulfur influences their electrocatalytic behavior.

Electrochemical characterization was carried out using rotating disk electrode and rotating ring-disk electrode techniques. These methods allow for a reliable assessment of intrinsic catalytic activity under well-controlled mass transport conditions, as well as the determination of reaction pathways and peroxide formation. The results obtained are discussed in relation to the structural features of the catalysts, with the aim of establishing clear structure-performance relationships.

The undoped Fe-N-C catalyst is first analyzed as a reference material. Subsequently, the impact of boron and sulfur incorporation is examined and compared to the baseline performance.

4.2 Electrochemical Activity of Undoped Fe-N-C

The undoped Fe-N-C catalyst was evaluated for its electrochemical performance as a baseline to compare the effect of heteroatom doping on the oxygen reduction reaction. The catalyst was thoroughly characterized as a reference material using cyclic voltammetry, linear sweep voltammetry, and rotating ring-disk electrode under alkaline and acidic conditions in terms of activity, kinetics, and selectivity.

4.2.1 Cyclic Voltammetry (CV) Analysis

The basic electrochemical principles of the undoped Fe-N-C catalyst investigated by cyclic voltammetry will provide an initial indication of the catalyst's activity for the oxygen reduction reaction. The experiments performed using nitrogen (N_2) or oxygen (O_2) saturated electrolyte, as well as in both acidic and basic environments allow for the identification of the reduction features of the ORR and give an indication of the stability of the catalyst/electrolyte interface and the capacitative properties of the catalyst.

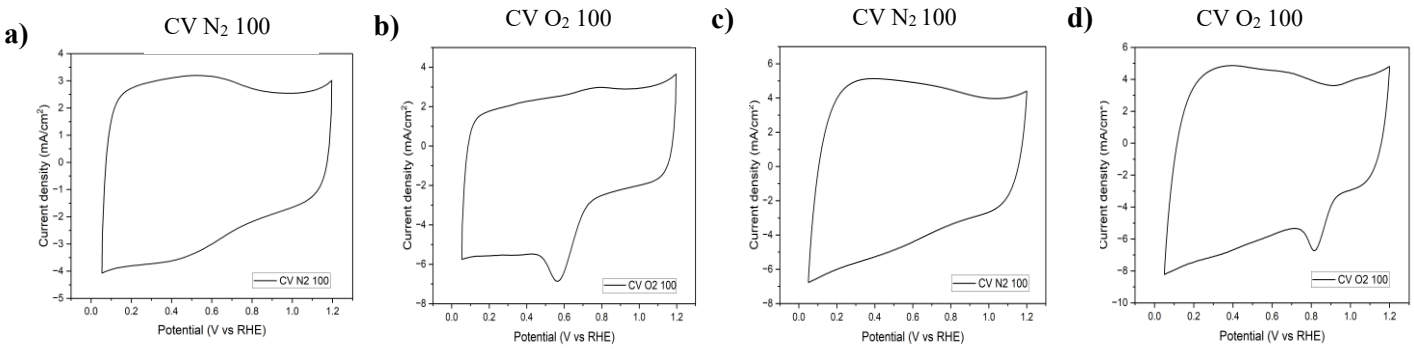

Fig. 4.1 Cyclic voltammetry of the Fe-N-C sample in both acidic (a, b) and alkaline (c, d) media at a scan rate of 100 mV s^{-1}.

Under N_2-saturated conditions (Fig. 4.1a and 4.1c), the curves display mainly capacitive behavior over the entire potential window, with no distinct redox peaks observed. The current densities range approximately from -4 to +3 mA cm^{-2} in acidic medium and from about -7 to +5 mA cm^{-2} in alkaline medium. This response is attributed to double-layer charging and confirms the electrochemical stability of the Fe-N-C electrode in both electrolytes. The higher capacitive current observed in alkaline medium suggests improved ionic conductivity and more effective charge transport in KOH.

When the electrolyte is saturated with O_2 (Fig. 4.1 b and d), a clear cathodic reduction feature appears within the potential range of approximately 0.8-0.4 V vs. RHE in acidic medium and 1- 0.7 V vs. RH in alkaline medium, corresponding to the oxygen reduction reaction. In acidic medium, the cathodic current reaches values close to -6 mA cm^{-2}, indicating measurable ORR activity. In alkaline medium, the reduction current is more pronounced, approaching -8 mA cm^{-2}, and occurs at slightly more positive potentials, demonstrating enhanced ORR kinetics. Overall, the CV results confirm that Fe-N-C is active toward oxygen reduction in both media, with superior performance observed in alkaline conditions.

4.2.2 Linear Sweep Voltammetry (LSV) Analysis

To quantitatively determine the ORR activity of the undoped Fe-N-C catalyst, linear sweep voltammograms were obtained using a rotating disk electrode. The three key performance parameters obtained from LSVs include onset potential, half-wave potential, and limiting current density. These measurements are crucial for assessing the intrinsic catalytic efficiencies of the catalyst, and also to facilitate comparison between both acidic and alkaline environments.

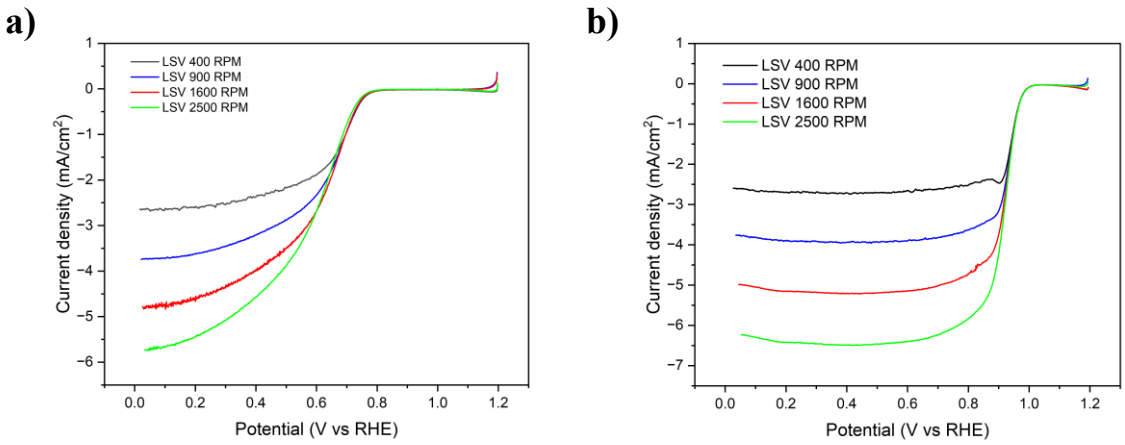

FIG 4.2 LSVs at different rotation rates (400, 900, 1600, and 2500 rpm) in both acid (a) and alkaline (b) electrolytic solutions for Fe-N-C.

The LSV polarization curves of the Fe-N-C catalyst at different rotation speeds (400-2500 rpm), as indicated by Figure 4.2, are shown for both acidic and alkaline solutions. In acidic conditions (4.2a), an increase in limiting current density occurs with increasing rotation speed from approximately -2.6 to about -5.8 mA cm^{-2}, indicating that oxygen mass transport has a significant effect. The onset potential for the ORR is about 0.70 - 0.75 V vs. RHE and is followed by a diffusion-limited plateau at potentials below approximately 0.50 V.

In alkaline solution (4.2b), the ORR is shifted to more positive potentials, with the onset occurring at approximately 0.90 - 1.00 V vs RHE. The limiting current density for the ORR reaches almost -6.5 mA cm^{-2} at 2500 rpm, indicating that the ORR activity of Fe-N-C has improved when compared to behavior in acidic solutions. The increase in current density with rotation rate in both media indicates that diffusion is controlling the behavior of Fe-N-C at low potentials, indicating that the ORR kinetic performance of Fe-N-C in an alkaline solution is superior.

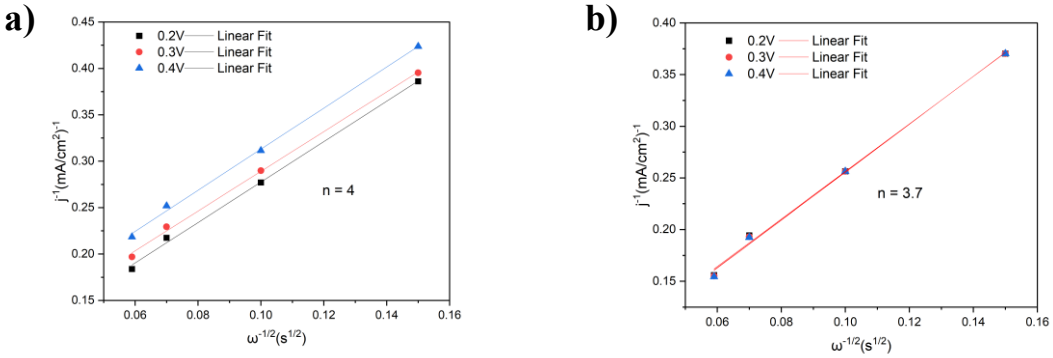

Fig. 4.3 The Koutecky-Levich plots at different electrode potentials of Fe-N-C in (a) 0.1 M $HClO_4$ and (b) 0.1 M KOH. Insets indicate the electron transfer number (n) derived from the KL slopes.

The effect of rotation speed on the LSV response of ORR kinetics was evaluated with The Koutecky-Levich (eq 2.1) analysis to further evaluate the ORR kinetics of Fe-N-C using polarization data collected at different rotation speeds. K-L plots are displayed in Figure 4.3 , where the current density at selected potentials (0.2, 0.3, or 0.4 V vs. RHE) is plotted against the rotation rate in both 0.1 M $HClO_4$ and in 0.1 M KOH. The K-L plots for both electrolytes showed good linearity with consistent fit, indicating that the measured current comprises contributions from both kinetics and diffusion-controlled processes, with oxygen transport exhibiting Levich behavior, as expected.

Apparent n was calculated from the slope of the K-L lines (eq 2.2). In 0.1 M $HClO_4$, Fe-N-C exhibits $n \approx 4$, indicating that the ORR occurs primarily through the four-electron pathway. In 0.1 M KOH, n is estimated to be $n \approx 3.7$; while this value is slightly less than 4, it indicates that the majority of the ORR through the four-electron pathway also has a minor contribution through the peroxide (two-electron) pathway. The K-L analysis supports the conclusion that Fe-N-C has efficient ORR kinetics and excellent selectivity for the four-electron pathway and is thus a suitable benchmark for studies of doped samples.

4.2.3 Oxygen Reduction Reaction (ORR) Pathway Analysis

Undoped Fe-N-C catalyst was evaluated using a rotating ring-disk electrode to determine the mechanism of the oxygen reduction reaction. This technique helps establish the electron transfer number and the amount of hydrogen peroxide produced in the reaction. Analysis of both disk and ring currents will allow assessment of whether the oxygen reduction reaction occurs via the four-electron or two-electron mechanism(s).

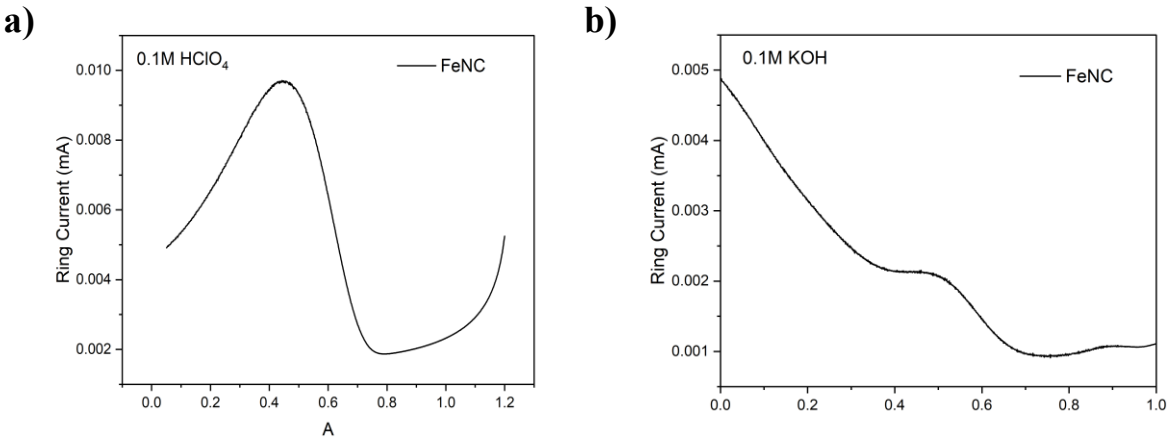

Fig. 4.4 Ring currents measured in (a) acidic and (b) alkaline media at 1600 RPM using a four-electrode setup for Fe-N-C

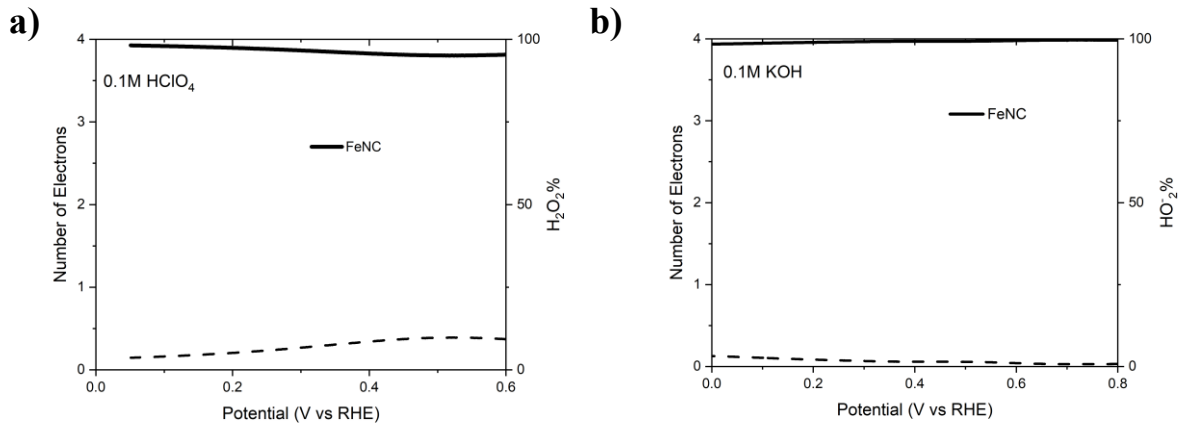

Fig. 4.5 ORR selectivity by RRDE measurement in a) acidic and b) alkaline environments for Fe-N-C.

Figure 4.5 shows further investigations of the Fe-N-C materials ORR selectivity using RRDE in acidic (0.1 M $HClO_4$) and alkaline (0.1 M KOH) conditions. In the acidic electrolyte, shown in Figure 3.5a, the average number of electrons transferred per molecule of oxygen (*n*) remains approximately 3.8-4.0 throughout the potential region investigated (0.0 V to 0.6V vs. RHE), indicating that the reaction is occurring through a four-electron transfer pathway. This is also supported through a low dissolved H_2O_2 yield (approximately <10%), suggesting that the reaction is highly selective for producing only water.

In alkaline conditions, shown in Figure 4.5 b, *n* is still close to 4.0 (greater than 0.8 V vs. RHE), while the dissolved H_2O_2 yield is almost 0% in the higher potential range. Therefore, the findings show that Fe-N-C is highly selective for the direct four-electron transfer process for the reduction of oxygen to water in both acidic and alkaline media with only slightly improved selectivity when in alkaline conditions. The relatively low hydrogen peroxide yield demonstrates that the catalytic effectiveness of Fe-N_x sites are responsible for facilitating O-O bond breaking in an efficient manner.

4.2.4 Stability Test

The stability of the Fe-N-C catalyst was evaluated by chronoamperometric measurements at 0.68 V for 4 hours in both alkaline (0.1M KOH) and acidic (0.1M $HClO_4$) electrolytes (Fig. 4.6).

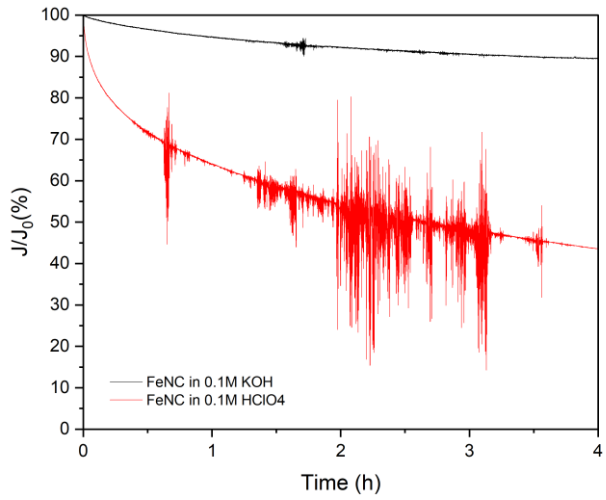

Fig. 4.6 i-t curves for FeNC achieved at 0.68 V in both acidic and alkaline media.

As shown in Fig. 4.6, Fe-N-C exhibits significantly higher stability under alkaline conditions. After 4 hours of continuous operation, the catalyst retains approximately 88-90% of its initial current density in 0.1M KOH, indicating relatively slow performance degradation. In contrast, in acidic medium the current density decreases more rapidly, dropping to nearly 45% of its initial value after 4 hours.

The reduced stability in acidic conditions can be attributed to the intrinsic vulnerability of Fe-N-C catalysts in proton-rich environments. Possible degradation mechanisms include dissolution of Fe-based active sites, carbon corrosion, and the formation of reactive peroxide intermediates that accelerate catalyst deterioration. These processes contribute to the substantial loss of catalytic activity over time.

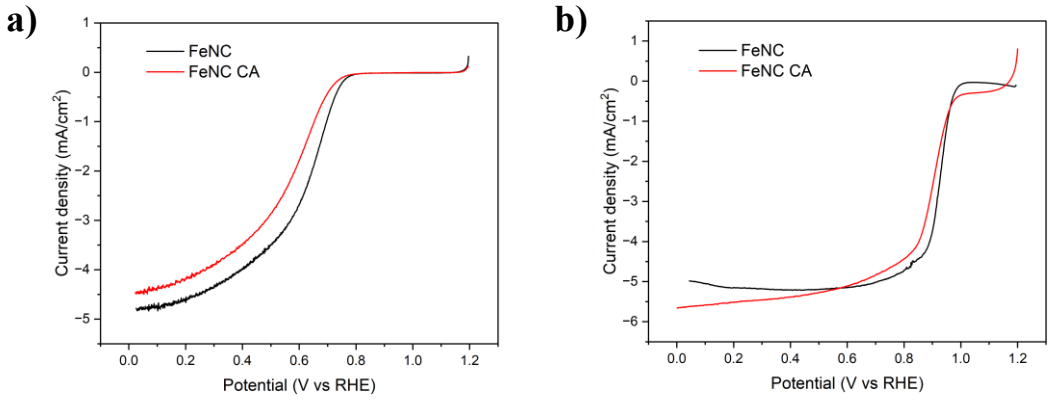

Fig. 4.7 LSV curves of FeNC recorded at 1600 rpm before (FeNC) and after (FeNC CA) the chronoamperometry (CA) stability test in both acidic (a) and alkaline (b) media.

Table 4.1 Onset and halfwave potentials for the proposed sample obtained from the LSV curves in 0.1M $HClO_4$.

	FeNC	FeNC CA
Onset Potential [V]	0.75	0.73
Half-wave Potential [V]	0.62	0.57

Table 4.2 Onset and halfwave potentials for the proposed sample obtained from the LSV curves in 0.1M KOH

	FeNC	FeNC CA
Onset Potential [V]	0.97	0.96
Half-wave Potential [V]	0.92	0.89

To assess the impact of prolonged operation on catalytic performance, LSV curves were recorded at 1600 rpm before and after the 4-hour chronoamperometric test in both acidic and alkaline media (Fig. 4.7). The corresponding onset and half-wave potentials extracted from the polarization curves are reported in Tables 4.1 and 4.2.

In acidic electrolyte (Fig. 4.7a), a noticeable deterioration in ORR activity is observed after the CA test. The onset potential shifts from 0.75 V to 0.73 V, while the half-wave potential decreases more significantly from 0.62 V to 0.57 V. This negative shift in the kinetic region indicates a loss of intrinsic catalytic activity, consistent with degradation of Fe-N_x active sites during prolonged exposure to the acidic environment. The reduced half-wave potential suggests a slower reaction kinetics after stability testing, confirming the substantial current decay observed in the chronoamperometric measurement.

In contrast, in alkaline electrolyte (Fig. 4.7b), the changes are less pronounced. The onset potential decreases slightly from 0.97 V to 0.96 V, and the half-wave potential from 0.92 V to 0.89 V. Although a minor decline in activity is detectable, the overall shape of the polarization curves remains similar before and after the CA test, indicating that the catalyst structure is largely preserved under alkaline conditions.

These results further support the higher stability of Fe-N-C under alkaline conditions and its more pronounced degradation in acidic media.

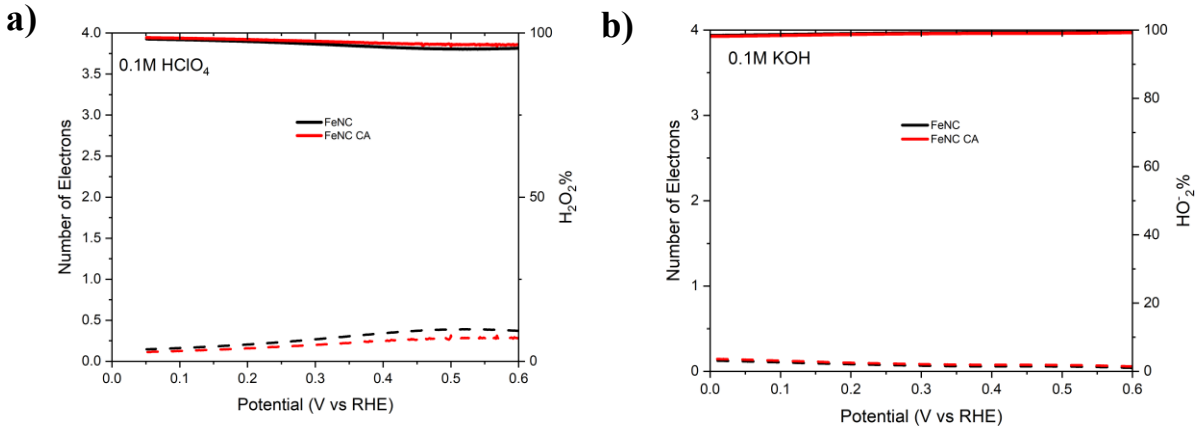

Fig. 4.8 ORR selectivity by RRDE measurement of Fe-N-C before (FeNC) and after (FeNC CA) the CA test, measured in both acidic (a) and alkaline (b) media.

To evaluate the effect of prolonged operation on ORR selectivity, RRDE measurements were performed before and after the 4-hour chronoamperometric test in both acidic and alkaline electrolytes (Fig. 4.8). The electron transfer number (*n*) and corresponding H_2O_2 yield were analyzed to assess possible changes in the reaction pathway.

In acidic environment (Fig. 4.8a), the number of electrons transferred slightly decreases through the CA test as $n \approx 4$ stays near the original value; however, at lower potentials, there is a slight downward deviation from the initial electron transfer number. With respect to this, there is a moderate increase in H_2O_2 yield when comparing before and after the stability test. This trend would indicate some loss of selectivity towards direct 4-electron pathways, which would be consistent with previous LSV results showing degradation of active Fe-N_x sites. The increased production of peroxides appears to be consistent with the results, suggesting possible further modifications to structural or chemical properties of the active sites during the extended operation time in acidic conditions, affecting the efficiency of oxygen reduction.

On the other hand, when tested under alkaline conditions (Figure 4.8b), the electron transfer number remains very close to 4 before and after the CA test, with negligible variation across the investigated potential range. The H_2O_2 yield remains minimal and nearly unchanged, indicating that the ORR pathway is preserved during prolonged operation.

Overall, the RRDE analysis before and after the CA test demonstrates that acidic conditions not only reduce catalytic activity but also slightly affect ORR selectivity, whereas alkaline conditions allow both activity and selectivity to remain substantially stable.

4.2.5 Discussion

The undoped Fe-N-C catalyst was systematically investigated as a benchmark material to establish a reference framework for evaluating the influence of heteroatom doping on ORR performance. The combined electrochemical analyses, including CV, LSV, Koutecký-Levich, RRDE, and durability testing, provide a comprehensive understanding of its activity, kinetics, selectivity, and stability in both acidic and alkaline electrolytes.

Cyclic voltammetry measurements reveal predominantly capacitive behavior under N_2-saturated conditions, indicating electrochemical stability of the Fe-N-C electrode and the absence of significant parasitic redox processes within the investigated potential window. The higher capacitive current observed in alkaline electrolyte suggests improved ionic conductivity and interfacial charge transport in KOH compared to $HClO_4$. Upon O_2 saturation, a clear cathodic reduction feature emerges in both media, confirming catalytic activity toward ORR. Notably, the reduction peak appears at slightly more positive potentials and with higher current density in alkaline medium, indicating enhanced ORR kinetics relative to acidic conditions.

The LSV analysis further quantifies this behavior. In acidic electrolyte, the ORR onset occurs around 0.70–0.75 V vs RHE, followed by a diffusion-limited plateau below approximately 0.50 V. The limiting current density increases systematically with rotation rate, demonstrating the strong contribution of oxygen mass transport. In alkaline medium, the ORR wave shifts toward more positive potentials (onset ≈ 0.90-1.00 V vs RHE), and higher limiting current densities are achieved, reflecting improved apparent activity. The consistent increase in limiting current with rotation speed in both electrolytes confirms diffusion-controlled behavior at low potentials and validates the applicability of Levich theory.

Koutecký-Levich analysis indicates good linearity, confirming that the measured current comprises contributions from both kinetic and diffusion-controlled processes. The calculated electron transfer number is close to four in acidic medium ($n \approx 4$), demonstrating that ORR predominantly follows a direct four-electron reduction pathway. In alkaline electrolyte, n is slightly lower (≈ 3.7), suggesting a minor contribution from the two-electron peroxide pathway, although the four-electron process remains dominant. These findings establish Fe-N-C as an efficient ORR catalyst with high intrinsic selectivity.

RRDE measurements corroborate this interpretation. In acidic conditions, the average electron transfer number remains in the range of 3.8-4.0 across the investigated potentials, accompanied by low H_2O_2 yields (typically below ~10%), indicating strong selectivity toward water formation. In alkaline electrolyte, n approaches 4 with nearly negligible peroxide production, confirming superior selectivity under basic conditions. The low peroxide yield implies effective O-O bond cleavage facilitated by Fe-N_x active sites and supports the mechanistic conclusion drawn from KL analysis.

Despite its promising activity and selectivity, durability tests highlight a critical limitation of undoped Fe-N-C under acidic conditions. Chronoamperometric measurements show that in alkaline electrolyte the catalyst retains approximately 88–90% of its initial current after 4 hours, indicating relatively stable operation. In contrast, in acidic medium the current decreases to nearly 45% of its initial value, accompanied by fluctuations that suggest progressive degradation of active sites. Post-stability LSV measurements confirm this deterioration, with noticeable negative shifts in onset and half-wave potentials in acid, whereas only minor changes are observed in alkaline medium. RRDE analysis before and after stability testing further reveals that acidic degradation slightly increases peroxide formation, indicating partial loss of selectivity, while alkaline selectivity remains essentially unchanged.

The inferior acid stability can be attributed to the intrinsic vulnerability of Fe-N-C materials in proton-rich environments, where Fe-site dissolution, carbon corrosion, and the formation of reactive oxygen intermediates may accelerate degradation. Conversely, the milder alkaline environment mitigates these processes, preserving both activity and selectivity.

Overall, the undoped Fe-N-C catalyst demonstrates efficient ORR activity and high selectivity toward the four-electron pathway, particularly in alkaline electrolyte. However, its limited stability in acidic conditions underscores the necessity of structural and electronic modifications to enhance durability. This baseline behavior provides a crucial reference for assessing the impact of boron and sulfur doping on the catalytic performance, stability, and mechanistic properties of Fe-N-C-based electrocatalysts.

4.3 Electrochemical Activity of Undoped Fe-N-C vs Boron Doping Catalysts

The electrochemical performance of the undoped Fe-N-C catalyst was investigated to establish a benchmark for evaluating the effects of heteroatom doping on the ORR activity and kinetics. Measurements were performed in oxygen- and nitrogen-saturated electrolytes using RDE and RRDE setups, following the protocols described in Chapter 2.

4.3.1 Cyclic Voltammetry (CV) Analysis

Cyclic voltammetry measurements were first performed to evaluate the fundamental electrochemical behavior of the Fe-N-C catalyst and assess their ORR activity [FIG 4.9] This test was conducted under nitrogen-saturated and oxygen-saturated conditions according to the protocol depicted in Section 2.5.2 .

In N_2-saturated electrolyte, all samples exhibit mainly capacitive currents associated with double-layer charging, with no distinct redox peaks observed. This behavior indicates the absence of significant electrochemical reactions under inert conditions and confirms that the catalytic features observed under oxygen are related to the oxygen reduction reaction.

In O_2-saturated electrolyte, clear cathodic reduction features are observed for all catalysts, confirming their ORR activity. In both media, the ORR-related features appear at more positive potentials in alkaline electrolyte than in acidic electrolyte, consistent with faster ORR kinetics in alkaline conditions. [46]

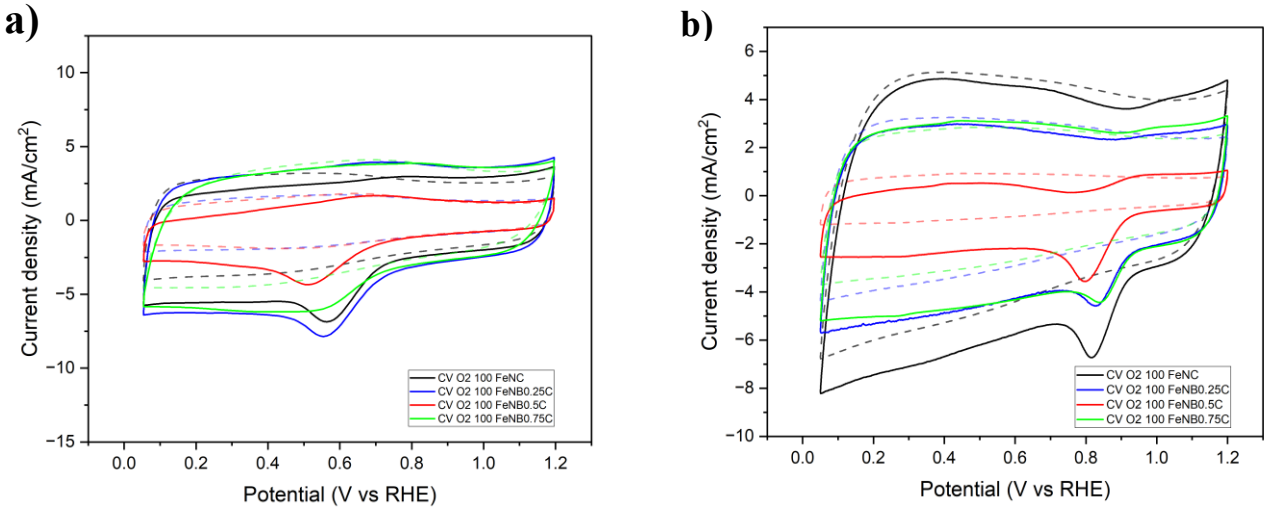

Fig. 4.9 Cyclic voltammetry of the samples in O_2-saturated electrolyte (solid lines) and N_2-saturated electrolyte (dashed lines) in both a) acidic and b) alkaline media.

Using Fe-N-C as the reference catalyst, the ORR response of the boron-doped samples shows a strong dependence on boron content. In acidic medium, $FeNB_{0.25}C$ exhibits a more pronounced ORR reduction feature and higher cathodic current density than Fe-N-C, indicating enhanced ORR activity at low boron content. In contrast, $FeNB_{0.5}C$ shows the weakest ORR response, while $FeNB_{0.75}C$ displays intermediate behavior. In alkaline medium, Fe-N-C shows the highest current density and most evident ORR features, whereas all boron-doped samples exhibit lower activity, with $FeNB_{0.5}C$ again presenting the poorest performance.

Overall, the CV results demonstrate that boron doping affects ORR activity in a non-linear manner. Low boron incorporation can enhance ORR behavior in acidic medium, while higher or non-optimal boron contents lead to reduced activity, likely due to changes in the electronic structure, conductivity, and accessibility of Fe-N_x active sites.

4.3.2 Linear Sweep Voltammetry (LSV) Analysis

To analyze the activity of the synthesized Fe-N-C and boron-doped (FeNB0.25C, FeNB0.5C, and FeNB0.75C) catalysts for the oxygen reduction reaction (ORR), linear sweep voltammetry was performed at rotation rates of 400, 900, 1600 and 2500 rpm in acidic and alkaline electrolytes. Polarization curves obtained at 1600 rpm were used to evaluate the catalytic activity of all the catalysts, since this rotation speed is routinely used to evaluate ORR catalytic performance under standardized mass-transport conditions. The onset potentials and half-wave potentials measured from the 1600 rpm polarization curves are summarized in Tables 4.3 and 4.4.

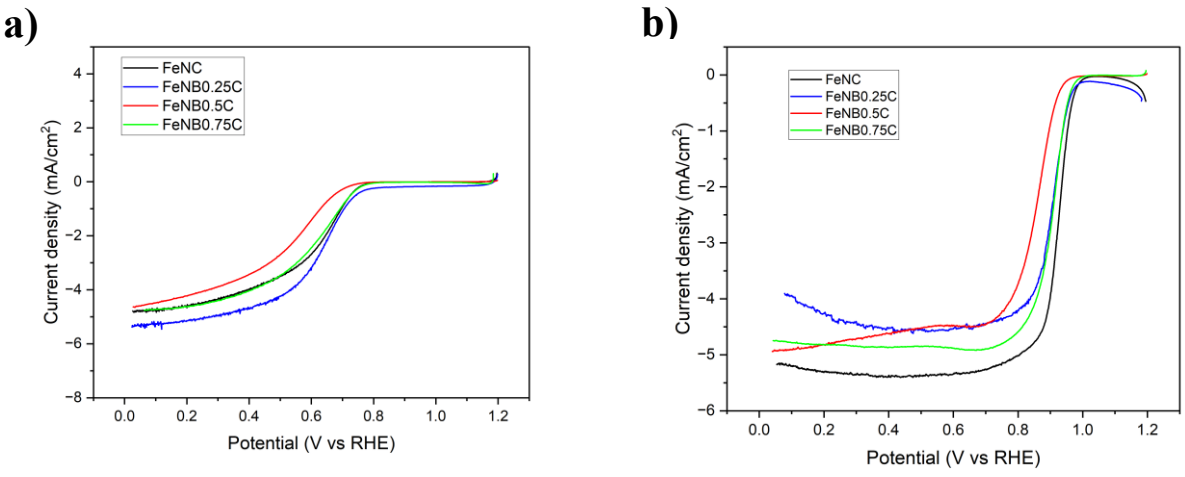

FIG 4.10 ORR electrocatalytic activity of the samples in both (a) acidic and (b) alkaline environments

Table 4.3 Onset and halfwave potentials for the proposed sample obtained from the LSV curves in 0.1M $HClO_4$.

	FeNC	$FeNB_{0.25}C$	$FeNB_{0.5}C$	$FeNB_{0.75}C$
Onset Potential [V]	0.74	0.75	0.7	0.76
Half-wave Potential [V]	0.62	0.63	0.55	0.6

Table 4.4 Onset and halfwave potentials for the proposed sample obtained from the LSV curves in 0.1M KOH

	FeNC	$FeNB_{0.25}C$	$FeNB_{0.5}C$	FeNB0.75C
Onset Potential [V]	0.97	0.96	0.93	0.96
Half-wave Potential [V]	0.92	0.9	0.85	0.9

In acidic medium, Fe-N-C is taken as the reference catalyst. The low-boron sample $FeNB_{0.25}C$ shows ORR behavior comparable to or slightly better than Fe-N-C, indicating that limited boron incorporation can preserve ORR kinetics. In contrast, $FeNB_{0.5}C$ exhibits a clear loss in activity, while $FeNB_{0.75}C$ shows intermediate performance, maintaining a competitive onset potential but without a consistent improvement over Fe-N-C across the full polarization range.

In alkaline medium, all catalysts display improved ORR behavior compared to acidic conditions. Fe-N-C exhibits the most favorable polarization profile, while $FeNB_{0.25}C$ and $FeNB_{0.75}C$ show slightly reduced activity. Again, $FeNB_{0.5}C$ presents the weakest ORR performance, confirming that intermediate boron content is detrimental in both electrolytes.

Overall, the LSV results indicate that boron doping affects ORR activity in a non-linear manner. Low boron incorporation maintains ORR performance, whereas intermediate boron content leads to systematic activity degradation, highlighting the importance of optimizing dopant concentration to balance electronic and transport properties of Fe-N-C catalysts.

Influence of the Rotation Rate

Within the Rotating Disk Electrode configuration, the effect of the electrode rotation rate provides valuable insight into the role of mass transport in the oxygen reduction reaction . By increasing the rotation speed enhances forced convection in the electrolyte, improving oxygen transport toward the catalyst surface and thereby influencing the measured current density.

FIG 4.11 shows the linear sweep voltammetry curves recorded at different rotation rates in both alkaline and acidic media, following the protocol described in Section 2.5.3. At higher potentials, the polarization curves obtained at different rotation speeds largely overlap, indicating that ORR kinetics are governed by charge-transfer processes and are only weakly affected by mass transport. As the potential decreases, the influence of rotation rate becomes increasingly evident, with the limiting current density rising systematically with increasing rotation speed. This behavior reflects enhanced oxygen availability at the electrode surface and is consistent with the Levich equation (eq 2.1) for diffusion-limited processes under forced convection.

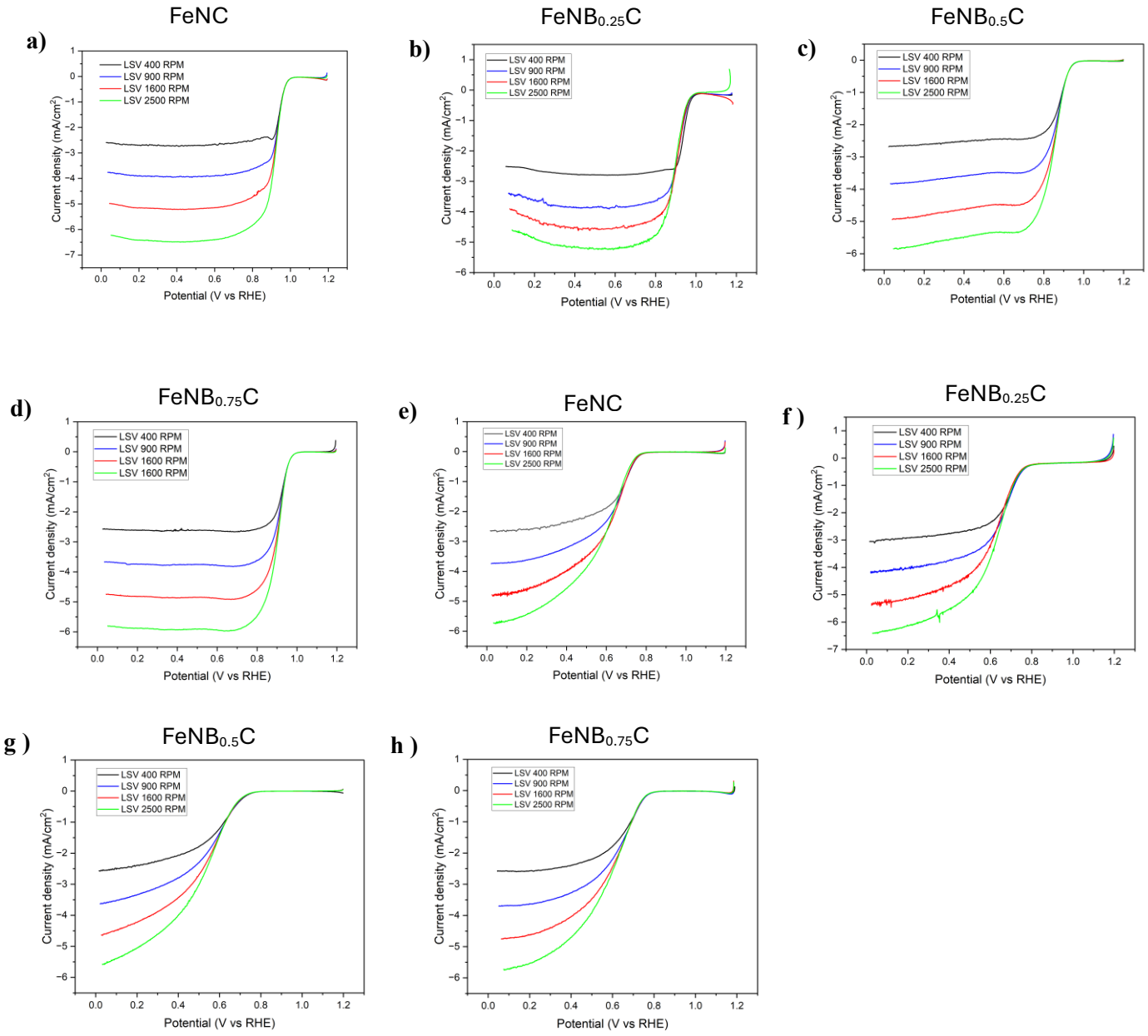

Fig. 4.11 LSVs at different rotation rates (400, 900, 1600, and 2500 rpm) in both alkaline (a, b, c, d) and acid (d, e, f ,g) electrolytic solutions for Fe-N-C, $FeNB_{0.25}C$, $FeNB_{0.5}C$, $FeNB_{0.75}C$

To quantitatively assess the impact of rotation rate on ORR kinetics, Koutecký-Levich analysis was performed. K-L plots, constructed by plotting 1/j as a function of $\omega^{-1/2}$, are shown in [FIG 4.12]. The analysis was carried out at selected potentials where mass transport effects are significant, namely 0.2, 0.3, and 0.4 V in alkaline and acidic media.

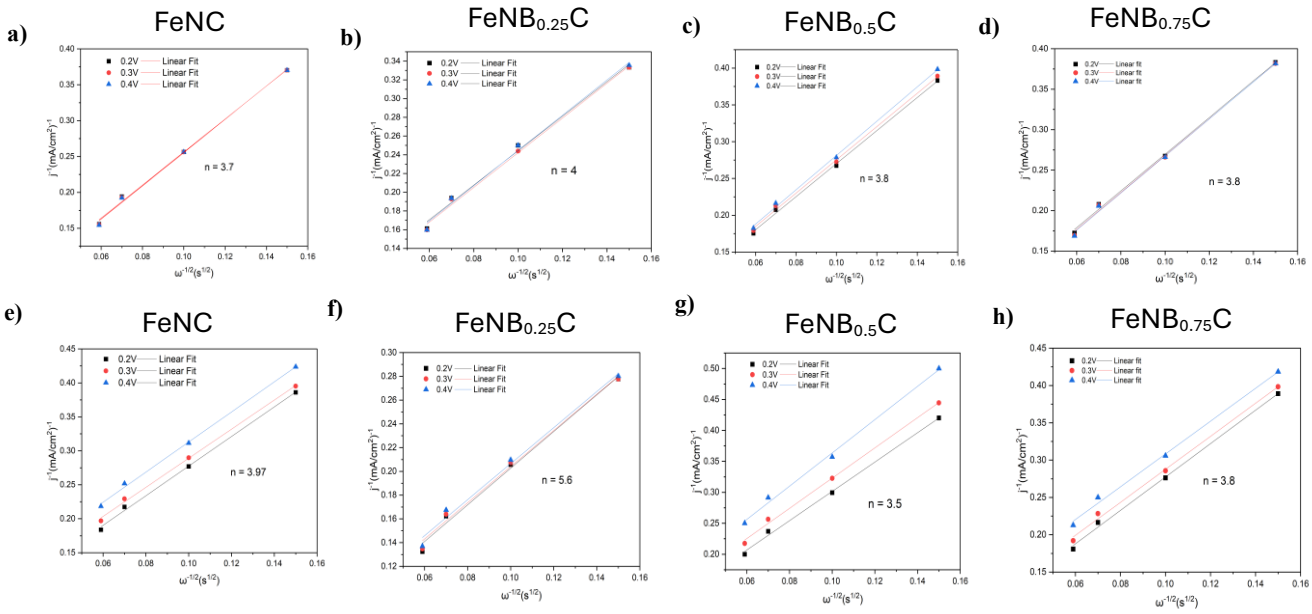

Fig. 4.12 The Koutecky-Levich plots at different electrode potentials of Fe-N-C, $FeNB_{0.25}C$, $FeNB_{0.5}C$, $FeNB_{0.75}C$ in (a, b, c, d) 0.1 M KOH and (e, f, g , h) 0.1 M $HClO_4$. Insets indicate the electron transfer number (*n*) derived from the K-L slopes.

rom the slopes of the Koutecký-Levich plots, the electron transfer number during ORR was extracted. For Fe-N-C, $FeNB_{0.25}C$, $FeNB_{0.5}C$, and $FeNB_{0.75}C$, the calculated electron transfer numbers are close to four in both acidic and alkaline media ($n \approx 4$) for all Fe-N-C-based catalysts, indicating that the ORR predominantly follows a direct four-electron pathway. This result confirms the high selectivity of the catalysts toward water formation and supports their potential applicability in fuel cell systems.

4.3.3 Oxygen Reduction Reaction (ORR) Pathway Analysis

To better understand the ORR mechanism, rotating ring-disk electrode measurements were conducted to assess the selectivity of the synthesized catalysts toward the four-electron reduction pathway. The analysis followed the procedure described in Section 2.5.1 , using Equations (2.3) and (2.4) to determine the electron transfer number during

ORR and the corresponding hydrogen peroxide yield. All RRDE tests were performed at a constant rotation speed of 1600 rpm.

The ring currents measured in both acidic and alkaline electrolytes are reported in Fig. 4.13. In an RRDE configuration, hydrogen peroxide produced at the disk electrode during ORR is transported to the ring electrode, where it is oxidized at a suitable applied potential, as detailed in the protocol described in Section 2.5.1 . Consequently, the ring current provides a direct indication of peroxide formation and, therefore, of the selectivity of the ORR pathway.

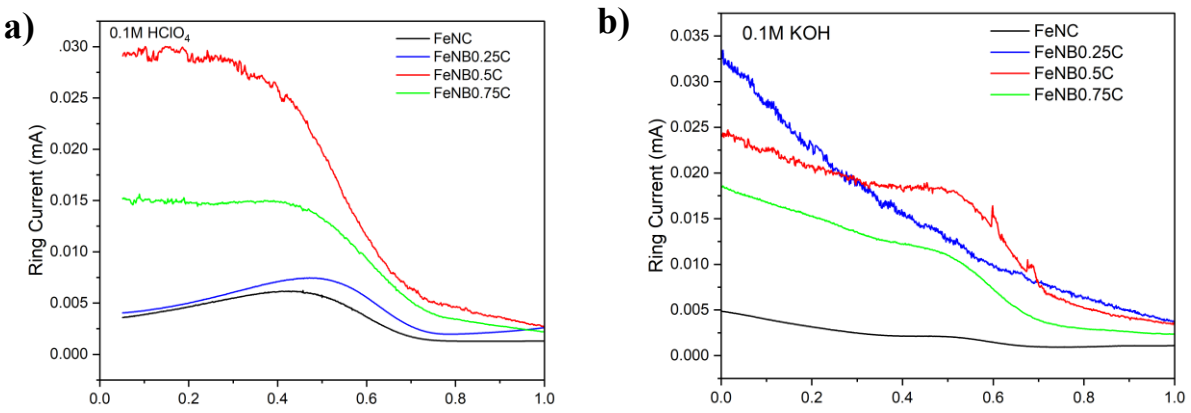

Fig. 4.13 Ring currents measured in (a) acidic and (b) alkaline media at 1600 RPM using a four-electrode setup.

In 0.1M $HClO_4$ (Fig. 4.13a), $FeNB_{0.5}C$ exhibits the highest ring current, indicating the greatest peroxide production and therefore the lowest selectivity toward the four-electron pathway. $FeNB_{0.75}C$ shows intermediate ring currents, whereas Fe-N-C and $FeNB_{0.25}C$ display the lowest ring currents, confirming improved selectivity. In 0.1M KOH (Fig. 4.13b), all samples show reduced ring currents compared to acidic conditions, indicating better selectivity in alkaline medium. Fe-N-C maintains the lowest peroxide-related current, while $FeNB_{0.5}C$ again shows the highest value among the series.

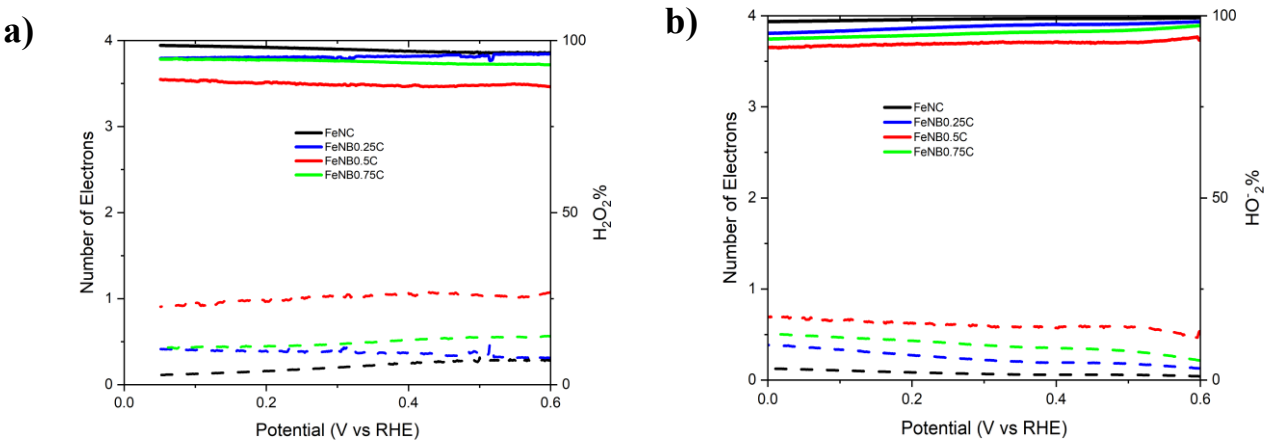

Fig. 4.14 ORR selectivity by RRDE measurement in a) acidic and b) alkaline environments.

Quantitative evaluations support previous conclusions made. Figure 4.14 displays that Fe-N-C has an electron transfer number of about four and produces the least amount of H_2O_2 in an acidic solution, indicating it primarily operates via a four-electron reaction. $FeNB_{0.25}C$ and $FeNB_{0.75}C$ are also primarily 4 electron catalysts but produce slightly more H_2O_2; while $FeNB_{0.5}C$ exhibited lower electron transfer numbers yet produced the largest amount of H_2O_2, indicating a more significant contribution from the two-electron route than the four-electron. All the catalysts reveal that they have an electron transfer number of approximately four for the alkaline solution and have reduced levels of peroxide yield formation. Among the four catalysts tested, Fe-N-C shows the lowest selectivity, whereas $FeNB_{0.5}C$ exhibits the highest selectivity for H_2O_2 production.

4.3.4 Stability Test

The CA curves (Fig. 4.15) reveal distinct differences between Fe-N-C and $FeNB_{0.25}C$, particularly in acidic electrolyte.

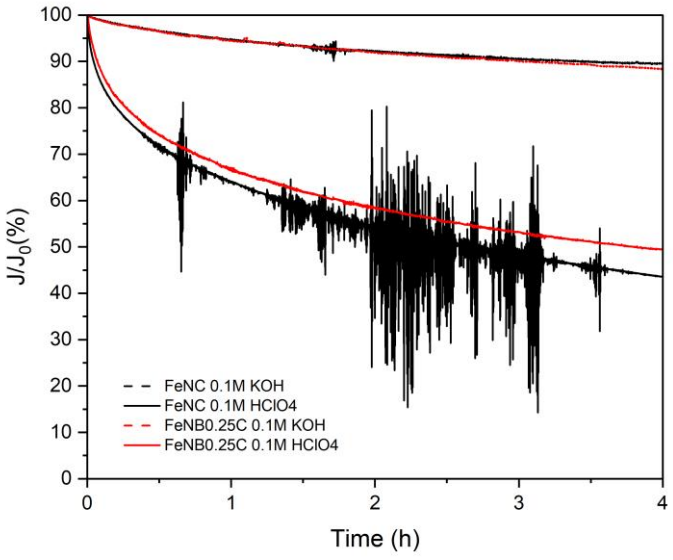

Fig. 4.15 i-t curves for FeNC and $FeNB_{0.25}C$ achieved at 0.68 V in both acidic (solid line) and alkaline (dash line) media.

In alkaline electrolyte, both catalysts display relatively stable current retention over the 4-hour test, maintaining close to 90% of their initial current density. The decay profiles are gradual and smooth, indicating that neither catalyst undergoes severe structural degradation in basic medium. This behavior confirms the inherent stability of Fe-N-C materials in alkaline environments and suggests that boron incorporation does not significantly alter the already favorable alkaline durability.

In acidic electrolyte, however, the degradation behavior is markedly different. Fe-N-C exhibits a rapid initial current drop followed by continuous decay, ultimately retaining less than half of its initial activity after 4 hours. The pronounced current fluctuations observed during the test indicate instability of the catalytic layer, likely associated with progressive degradation of Fe-N_x active sites and carbon corrosion.

In contrast, $FeNB_{0.25}C$ shows a noticeably slower rate of degradation and reduced fluctuation amplitude. Although performance loss still occurs, the boron-doped catalyst retains a higher fraction of its initial current compared to Fe-N-C. The smoother decay profile suggests improved structural integrity and more stable active site environments during prolonged operation in acidic medium.

This behavior indicates that boron incorporation enhances resistance against acid-induced degradation processes.

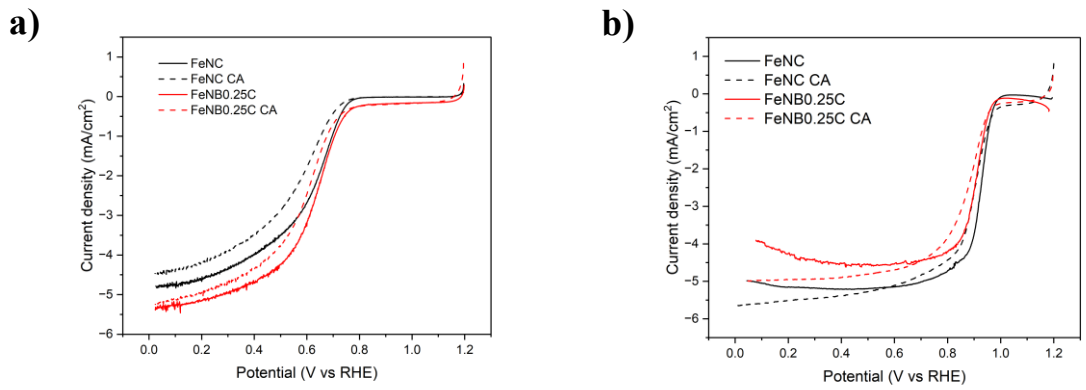

Fig. 4.16 LSV curves of FeNC and $FeNB_{0.25}C$ recorded at 1600 rpm before (FeN , $FeNB_{0.25}C$) and after (FeNC CA, , $FeNB_{0.25}C$ CA) the chronoamperometry (CA) stability test in both acidic (a) and alkaline (b) media.

Table 4.5 Onset and halfwave potentials for the proposed sample obtained from the LSV curves in 0.1M $HClO_4$.

	FeNC	FeNC CA	$FeNB_{0.25}C$	$FeNB_{0.25}C$ CA
Onset Potential [V]	0.75	0.73	0.75	0.73
Half-wave Potential [V]	0.62	0.57	0.63	0.6

Table 4.6 Onset and halfwave potentials for the proposed sample obtained from the LSV curves in 0.1M KOH

	FeNC	FeNC CA	$FeNB_{0.25}C$	$FeNB_{0.25}C$ CA
Onset Potential [V]	0.97	0.96	0.96	0.97
Half-wave Potential [V]	0.92	0.89	0.9	0.87

The impact of prolonged operation on intrinsic ORR kinetics is further elucidated by comparing LSV curves recorded before and after the CA test (Fig. 4.16).

In 0.1M $HClO_4$, Fe-N-C exhibits a noticeable negative shift in half-wave potential (from 0.62 V to 0.57 V), indicating substantial kinetic degradation. This shift reflects a decrease in intrinsic catalytic activity and suggests partial deactivation or loss of active Fe-N_x sites during acidic operation.

$FeNB_{0.25}C$ also shows a decline in activity; however, the decrease in half-wave potential is less pronounced (from 0.63 V to 0.60 V). The smaller kinetic shift indicates that boron doping mitigates activity loss under acidic conditions. Importantly, the similar onset potentials before and after testing suggest that the fundamental ORR mechanism is preserved, but the density or effectiveness of active sites is partially reduced.

In alkaline electrolyte, both catalysts exhibit only minor shifts in half-wave potential after CA testing. The overall polarization curves remain similar in shape and position, confirming that prolonged operation does not significantly alter the catalytic structure or intrinsic kinetics in basic medium.

These observations reinforce the conclusion that the stability challenge is primarily associated with acidic conditions and that boron doping provides measurable improvement in acid tolerance.

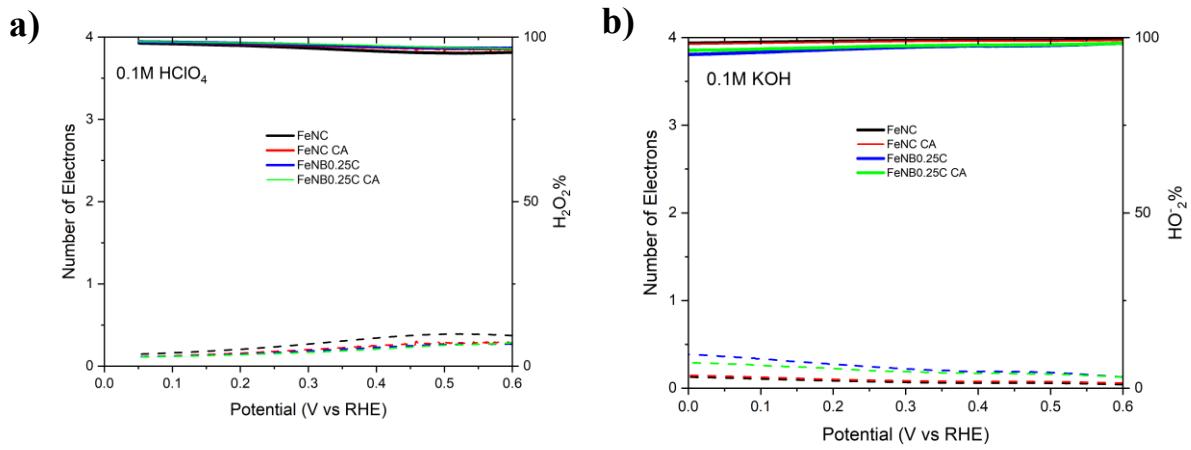

Fig. 4.17 ORR selectivity by RRDE measurement in Fe-N-C and $FeNB_{0.25}C$ before (FeNC , $FeNB_{0.25}C$) and after (FeNC CA , $FeNB_{0.25}C$ CA) the CA test, measured in both acidic (a) and alkaline (b) media.

RRDE measurements (Fig. 4.17) provide further insight into how durability influences ORR selectivity.

In acidic medium, Fe-N-C shows a slight decrease in the electron transfer number after CA testing, accompanied by an increase in H_2O_2 yield. This indicates that degradation

not only affects activity but also slightly compromises selectivity, allowing a greater contribution from the two-electron pathway. Such behavior suggests that structural deterioration of Fe-N_x sites may alter oxygen adsorption configurations and reduce the efficiency of O-O bond cleavage.

In contrast, $FeNB_{0.25}C$ maintains an electron transfer number closer to four even after prolonged operation, with only a minor increase in peroxide yield. This stability in selectivity suggests that boron incorporation helps preserve the integrity of the active sites responsible for facilitating the direct four-electron reduction pathway.

In alkaline electrolyte, both catalysts retain n values very close to 4 before and after CA testing, with negligible peroxide production. This confirms that the ORR pathway remains unchanged and highly selective in basic conditions, consistent with the minimal activity loss observed in LSV measurements.

Overall, while both catalysts exhibit strong stability in alkaline electrolyte, the boron-doped $FeNB_{0.25}C$ demonstrates improved resistance to acid-induced degradation compared to undoped Fe-N-C. The enhanced durability is reflected not only in higher current retention but also in reduced kinetic loss and better preservation of ORR selectivity.

These results indicate that boron incorporation provides a beneficial effect on both activity retention and mechanistic stability under harsh acidic conditions, highlighting its potential role in improving the long-term applicability of Fe-N-C catalysts in proton-exchange membrane fuel cell environments.

4.3.5 Discussion

The comparative electrochemical evaluation of undoped Fe-N-C and boron-doped Fe-N-C catalysts provides clear insight into how boron incorporation modulates ORR activity, kinetics, selectivity, and durability. Using Fe-N-C as a benchmark, the influence of boron content was systematically assessed through CV, LSV, rotation-rate studies, RRDE analysis, and chronoamperometric stability tests in both acidic and alkaline media.

Cyclic voltammetry under N_2 saturation shows mainly capacitive behavior for all samples, confirming the electrochemical stability of the carbon framework and the absence of parasitic redox processes. Under O_2 saturation, distinct cathodic reduction features are observed, confirming ORR activity. In both media, ORR-related features appear at more positive potentials in alkaline electrolyte, reflecting more favorable kinetics in KOH. The effect of boron is non-linear: in acidic medium, the low-boron sample ($FeNB_{0.25}C$) displays ORR behavior comparable to or slightly improved relative to Fe-N-C, suggesting that limited boron incorporation beneficially modifies the electronic structure of Fe-N_x active sites. In contrast, $FeNB_{0.5}C$ shows a clear loss in activity, with a negative shift in half-wave potential, while $FeNB_{0.75}C$ exhibits

intermediate performance. In alkaline medium, Fe-N-C maintains the most favorable polarization profile, whereas boron-doped samples, especially $FeNB_{0.5}C$, show slightly reduced activity. These results indicate that moderate boron incorporation can preserve ORR kinetics, but excessive or non-optimal doping perturbs active site accessibility or electronic structure.

Rotation-rate experiments and Koutecký-Levich analysis confirm that the limiting current increases with rotation speed, consistent with diffusion-controlled behavior at low potentials. The linear K-L plots and electron transfer numbers close to four in both electrolytes demonstrate that all catalysts predominantly follow the direct four-electron reduction pathway. Thus, boron doping does not alter the ORR mechanism but rather modulates intrinsic kinetics.

RRDE measurements further clarify selectivity. In acidic medium, $FeNB_{0.5}C$ exhibits the highest ring current and peroxide yield, indicating lower selectivity toward the four-electron pathway. $FeNB_{0.25}C$ and $FeNB_{.075}C$ show reduced peroxide production, comparable to Fe-N-C. In alkaline electrolyte, ring currents decrease significantly for all samples and electron transfer numbers approach four, confirming improved selectivity in KOH. The higher H_2O_2 formation for $FeNB_{0.5}C$ suggests that intermediate boron content may weaken O-O bond activation or disturb optimal adsorption configurations.

Chronoamperometric stability tests reveal that both Fe-N-C and $FeNB_{0.25}C$ exhibit high current retention in alkaline medium, indicating good durability in KOH. In acidic electrolyte, more pronounced degradation is observed, consistent with Fe-N-C vulnerability to demetallation and peroxide-induced carbon corrosion. Notably, $FeNB_{0.25}C$ maintains slightly higher residual current and reduced fluctuations compared to Fe-N-C, suggesting that appropriate boron incorporation may enhance structural stability of the carbon matrix and partially protect $Fe\text{-}N_x$ sites. Post-CA LSV and RRDE analyses show moderate shifts in half-wave potential and a slight increase in peroxide yield, yet the four-electron pathway remains dominant, indicating preservation of the fundamental reaction mechanism.

Overall, boron doping exerts a concentration-dependent effect on ORR performance. Low boron incorporation ($FeNB_{0.25}C$) achieves a favorable balance between activity, selectivity, and durability, whereas intermediate content ($FeNB_{0.5}C$) compromises both kinetics and selectivity. Across all samples, the ORR proceeds predominantly via the four-electron pathway, confirming that boron primarily influences electronic properties and stability rather than changing the reaction mechanism. These findings highlight the importance of dopant optimization in Fe-N-C catalysts and provide guidance for designing efficient and durable non-precious metal electrocatalysts for fuel cell applications.

4.4 Electrochemical Activity of Undoped Fe-N-C vs Sulfur Doping Catalysts

The electrochemical performance of sulfur-containing Fe-N-C catalyst has been analyzed and compared with that of an undoped Fe-N-C catalyst. The sulfur (theoura) was added during the preparation of the Fe-N-C catalyst in order to change the electronic structure of the active Fe-N_x site so as to enhance the catalytic activity of these sites for the oxygen reduction reaction. To evaluate the influence of sulfur content, three sulfur-doped catalysts with different sulfur loadings, namely $FeNS_{0.25}C$, $FeNS_{0.5}C$, and $FeNS_{0.75}C$, were synthesized and analyzed.

4.4.1 Cyclic Voltammetry (CV) Analysis

Cyclic voltammetry was conducted in nitrogen-saturated and oxygen-saturated electrolytes to evaluate the electrochemical behavior and ORR activity of the undoped Fe-N-C and sulfur-doped catalysts ($FeNS_{0.25}C$, $FeNS_{0.5}C$, and $FeNS_{0.75}C$), as shown in Fig. 4.18, in both acidic and alkaline media.

Under N_2-saturated conditions (dashed lines), all samples mainly exhibit capacitive currents associated with electrochemical double-layer charging, with no pronounced faradaic peaks. This confirms that no significant redox processes occur in the absence of oxygen and that the cathodic features observed under O_2 are attributable to ORR. Variations in the capacitive current among the samples may be related to differences in surface area, defect density, and surface functionality introduced by sulfur incorporation.

In O_2-saturated electrolyte, all catalysts display a well-defined cathodic reduction peak corresponding to the ORR process. In acidic medium (0.1 M $HClO_4$), the cathodic peak for Fe-N-C appears in the potential range of approximately 0.47–0.69 V vs RHE. The sulfur-doped samples exhibit similar but slightly shifted peak positions, with $FeNS_{0.25}C$ and $FeNS_{0.5}C$ showing reduction features between 0.48-0.70 V, while $FeNS_{0.75}C$ presents a more positively extended peak range of about 0.5-0.72 V. The slight positive shift and broader peak observed for FeNS0.75C suggest improved ORR activity at higher sulfur content under acidic conditions.

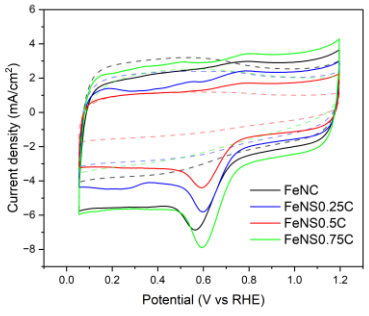

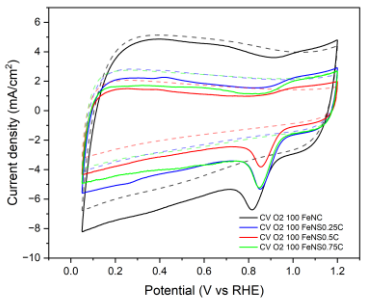

Fig. 4.18 Cyclic voltammetry of the samples in O_2-saturated electrolyte (solid lines) and N_2-saturated electrolyte (dashed lines) in both a) acidic and b) alkaline media

In alkaline medium (0.1 M KOH), the cathodic peaks shift to more positive potentials, indicating more favorable ORR kinetics. The reduction peak of Fe-N-C is observed between approximately 0.73-0.90 V vs RHE. The sulfur-doped samples exhibit peaks in the range of 0.79-0.93 V, showing a noticeable positive shift compared to acidic conditions. This confirms the enhanced ORR kinetics in alkaline electrolyte. However, despite the shift, Fe-N-C maintains a strong and stable reduction feature, suggesting that sulfur incorporation does not lead to a systematic improvement in alkaline medium.

Overall, the CV results demonstrate that sulfur doping influences the ORR behavior in a composition-dependent manner. Higher sulfur content appears beneficial in acidic medium, as reflected by the more positively shifted cathodic peak of $FeNS_{0.75}C$, whereas in alkaline medium the undoped Fe-N-C catalyst remains highly competitive.

4.4.2 Linear Sweep Voltammetry (LSV) Analysis

Linear sweep voltammetry measurements were performed at 1600 rpm in both acidic (0.1M $HClO_4$) and alkaline (0.1M KOH) electrolytes to evaluate the ORR activity of Fe-N-C and sulfur-doped catalysts ($FeNS_{0.25}C$, $FeNS_{0.5}C$, and $FeNS_{0.75}C$). The corresponding polarization curves are shown in Fig. 3.19, while the extracted onset and half-wave potentials are summarized in Tables 4.7 and 4.8.

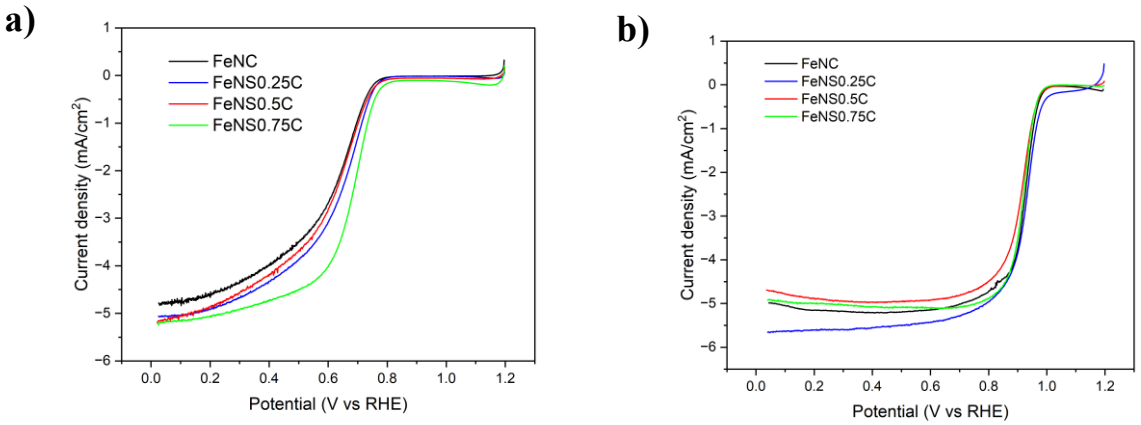

Fig. 4.19 ORR electrocatalytic activity of the samples in both (a) acidic and (b) alkaline environments

Table 4.7 Onset and halfwave potentials for the proposed sample obtained from the LSV curves in 0.1M $HClO_4$.

	FeNC	$FeNS_{0.25}C$	$FeNS_{0.5}C$	$FeNS_{0.75}C$
Onset Potential [V]	0.74	0.76	0.76	0.77
Half-wave Potential [V]	0.62	0.64	0.62	0.67

Table 4.8 Onset and halfwave potentials for the proposed sample obtained from the LSV curves in 0.1M KOH

	FeNC	$FeNS_{0.25}C$	$FeNS_{0.5}C$	$FeNS_{0.75}C$
Onset Potential [V]	0.97	0.98	0.97	0.97
Half-wave Potential [V]	0.92	0.92	0.91	0.92

All samples reveal standard ORR polarization characteristics in acidic electrolyte media and show similar diffusion-limited ORR current densities of approximately -5 mA/cm^2; therefore, they display similar mass transport characteristics. Conversely, in the kinetic region of the ORR polarization profiles differences became apparent based on sulfur content; specifically, incorporation of sulfur resulted in an increase in the onset potential from 0.74 V for the Fe-N-C catalyst to 0.77 V for the $FeNS_{0.75}C$catalyst and resulted in an increase of $E_{1/2}$ from 0.62 to 0.67 V; thus, it was indicated that higher sulfur loading improves the underlying kinetics of the ORR reaction. Sulfur loading contributed to a moderate enhancement of the $FeNS_{0.25}C$ catalyst, however the $FeNS_{0.5}C$ catalyst and Fe-N-C had virtually identical activities; consequently, there is no linear relationship between the degree of activity and sulfur loadings.

In alkaline electrolyte, all catalysts display improved ORR performance with closely overlapping polarization curves; however, $FeNS_{0.25}C$ exhibits a slightly more positive onset potential (0.98 V) compared to Fe-N-C (0.97 V), suggesting a modest enhancement in reaction initiation. The half-wave potentials remain nearly identical (~0.91- 0.92 V), indicating similar overall catalytic efficiency under alkaline conditions. The comparable limiting current densities in both media confirm that sulfur doping does not significantly affect oxygen diffusion, and that the observed differences arise mainly from intrinsic kinetic effects.

Influence of the Rotation Rate

As previously discussed in the earlier section on rotation rate analysis, increasing the electrode rotation speed enhances oxygen mass transport toward the catalyst surface due to forced convection in the RDE configuration. In the present case, this effect was evaluated for Fe-N-C and sulfur-doped catalysts in both alkaline and acidic electrolytes.

As shown in figure 4.20 of the LSV curves for the different sampling rates at 400, 900, 1600 and 2500 RPM, the high potential region of all the samples has a current density that is independent of the rotational speed suggesting that the ORR kinetics are limited to charge transfer. Additionally, as the potential drops, we see an increased effect of rotational speed with a systematic increase in limiting current density as the RPM are increased. This type of behaviour is characteristic of diffusion-controlled conditions and

is also consistent with the Levich model, which indicates that oxygen transport dominates the low potential region of the polarization curves.

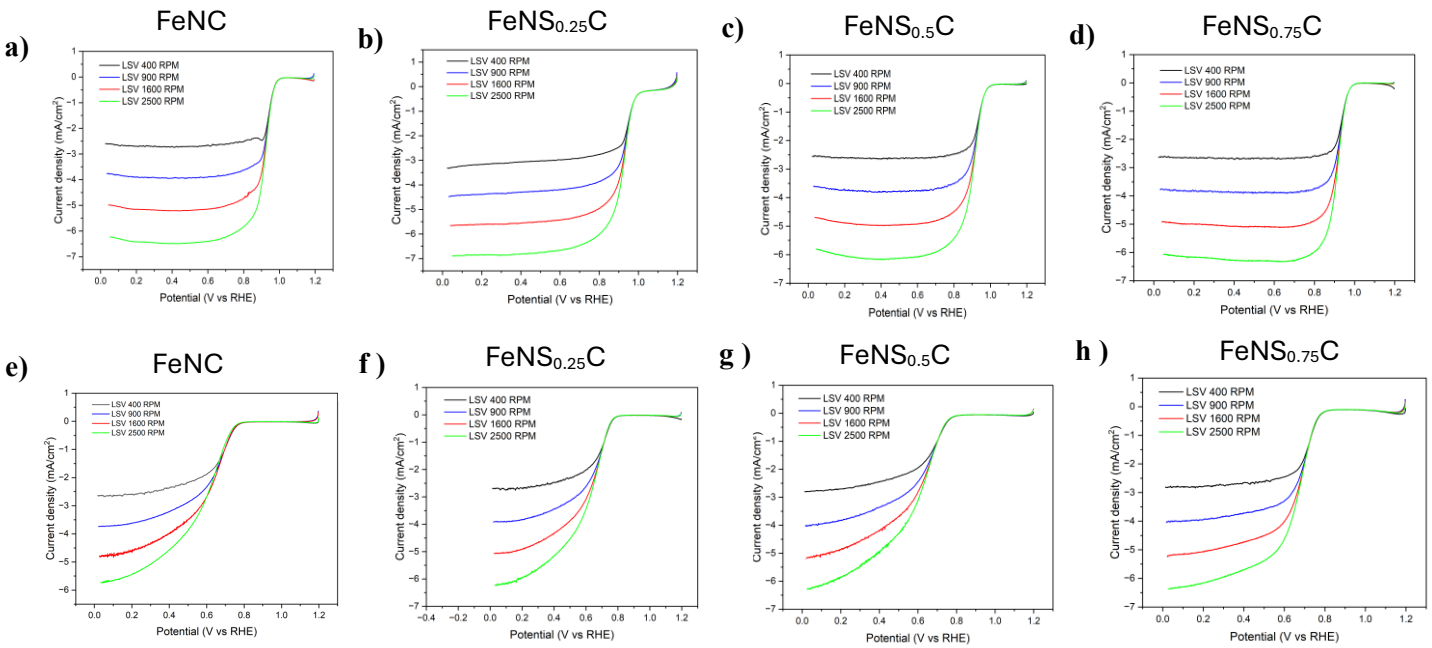

Fig. 4.20 LSVs at different rotation rates (400, 900, 1600, and 2500 rpm) in both alka- line (a, b, c, d) and acid (d, e, f ,g) electrolytic solutions for Fe-N-C, $FeNS_{0.25}C$, $FeNS_{0.5}C$, $FeNS_{0.75}C$

The close parallels between the limiting currents evolving with rotation rates for all of the catalysts demonstrate that incorporation of sulfur did not significantly change the mass transfer properties of the electrolyte in the catalyst layer. To more fully understand the ORR mechanism, Koutecký-Levich plots were made at selected potentials (see Fig. 4.21). The linearity of 1/j vs. $\omega^{-1/2}$ for both media suggests that the K-L method is valid to use for these measurements.

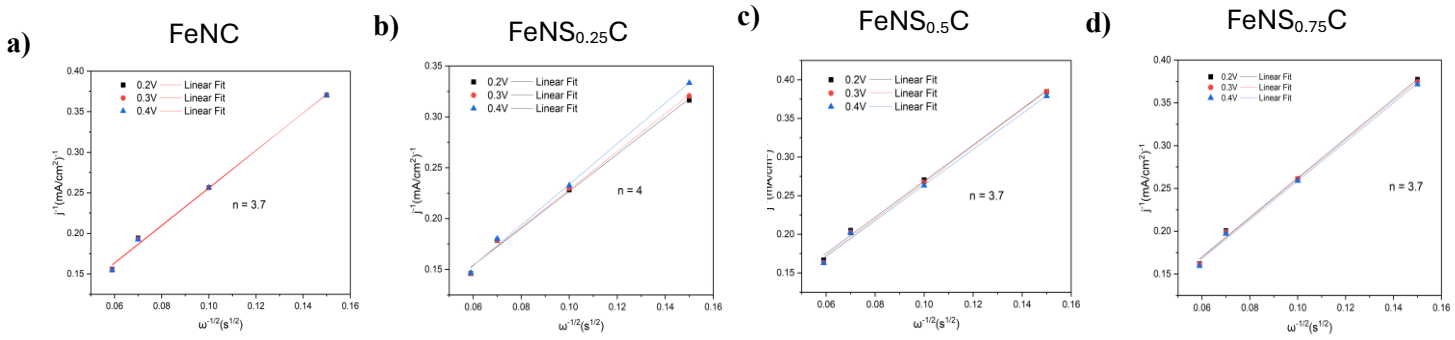

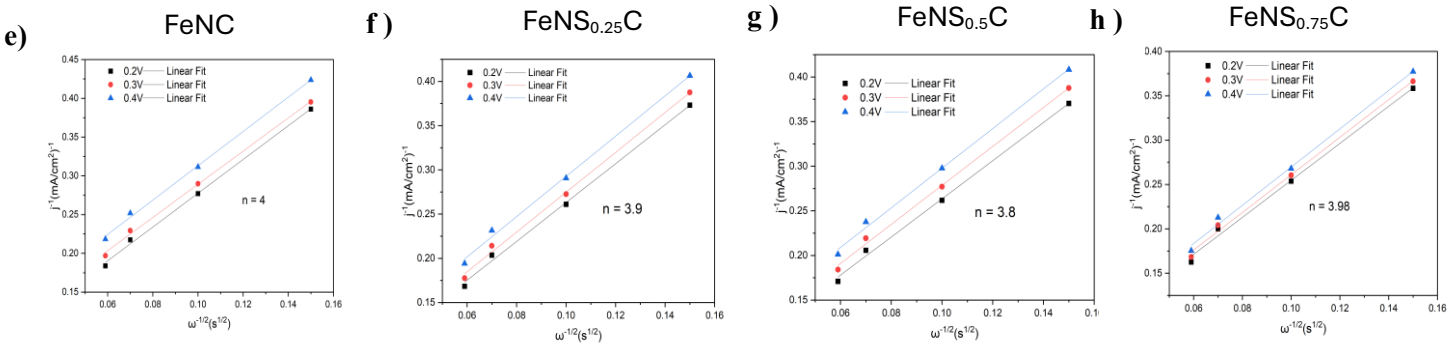

Fig. 4.21 The Koutecky-Levich plots at different electrode potentials of Fe-N-C, $FeNB_{0.25}C$, $FeNB_{0.5}C$, $FeNB_{0.75}C$ in (a, b, c, d) 0.1 M KOH and (e, f, g , h) 0.1 M $HClO_4$. Insets indicate the electron transfer number (*n*) derived from the KL slopes.

From the K-L slope, the electron transfer is close to four for all the samples. The electron transfer (*n*) values are around 3.7 - 4.0 in an alkaline electrolyte and are mostly close to 4 in an acidic medium. The four-electron reduction pathway seems to be the prevalent route for both undoped and sulfur-doped catalysts based on these results. The slight deviation from $n = 4$ indicates either slight differences in active site structure or surface properties of the catalyst and does not suggest any significant change to the ORR mechanism.

Overall, the rotation-rate experiment demonstrates that the way the ORR occurs does not change due to the incorporation of sulfur and that the selectivity towards a four-electron reduction continues to be very high.

4.4.3 Oxygen Reduction Reaction (ORR) Pathway Analysis

To gain further insight into the ORR mechanism and catalyst selectivity, rotating ring-disk electrode measurements were performed to evaluate the preference of Fe-N-C and sulfur-doped catalysts toward the four-electron reduction pathway. The disk and ring currents, required to calculate the electron transfer number (*n*) and the corresponding hydrogen peroxide yield (H_2O_2 %), are presented in Figures 4.22 and 4.23.

The ring current measured at 1600 rpm has been recorded for an acidic and alkaline medium in Figure 4.22 below. The ring current in an RRDE configuration is directly correlated to the amount of peroxide produced at the disk electrode, so lower ring current yields greater selectivity to the direct four-electron reduction pathway.

In addition, Fe-N-C has the lowest ring current throughout the entire range of potential studied, while $FeNS_{0.25}C$ yields the highest values; therefore, more peroxide is being produced at lower sulfur loadings with $FeNS_{0.25}C$ than with either of the other two materials ($FeNS_{0.5}C$ and $FeNS_{0.75}C$), which yield intermediate values between those two. Conversely, using an alkaline electrolyte, all of the materials tested have significantly lower ring currents than when an acidic electrolyte was used, thus

confirming that less peroxide was produced, thus making the ORR more selective when using an alkaline electrolyte as well. With regard to selectivity in the alkaline condition, once again Fe-N-C has the lowest ring current and $FeNS_{0.5}C$ and $FeNS_{0.75}C$ have ly larger ring currents, indicating they are less selective than Fe-N-C.

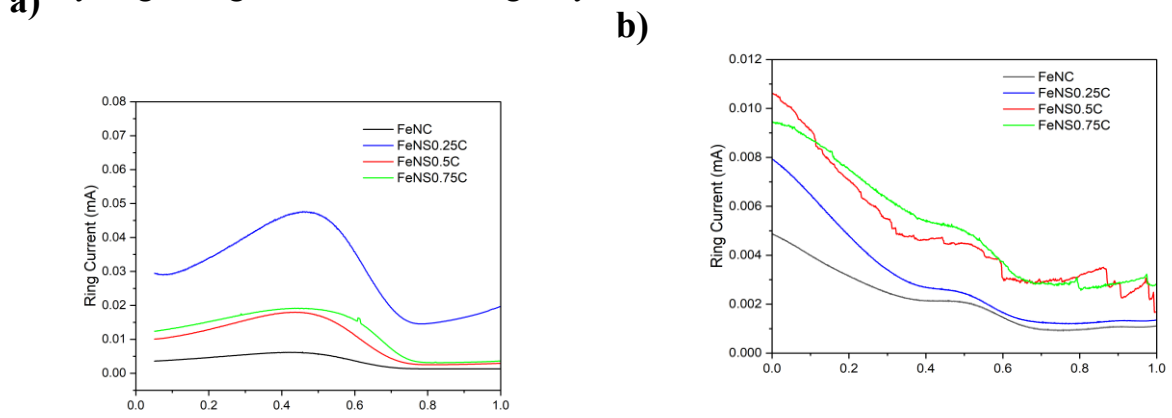

Fig. 4.22 Ring currents measured in (a) acidic and (b) alkaline media at 1600 RPM using a four-electrode setup.

The number of electrons transferred (n) and the amount of H_2O_2 produced were determined to quantitatively assess the ORR pathway (Figure 4.23). Fe-N-C shows essentially identical values of n (close to 4) throughout the potential range measured in acidic conditions, which means it mainly uses a four-electron pathway. The sulfur doped catalysts also exhibited n values close to 4, but $FeNS_{0.5}C$ and $FeNS_{0.75}C$ were both lower than 4, especially at lower potentials, which means that the amount of H_2O_2 produced was therefore moderate relative to Fe-N-C (but slightly higher). In alkaline conditions, all of the samples had n values close to 4 (3.9 to 4.0) and produced small amounts of H_2O_2 (generally < 1%), which indicates a preference for total reduction of oxygen.

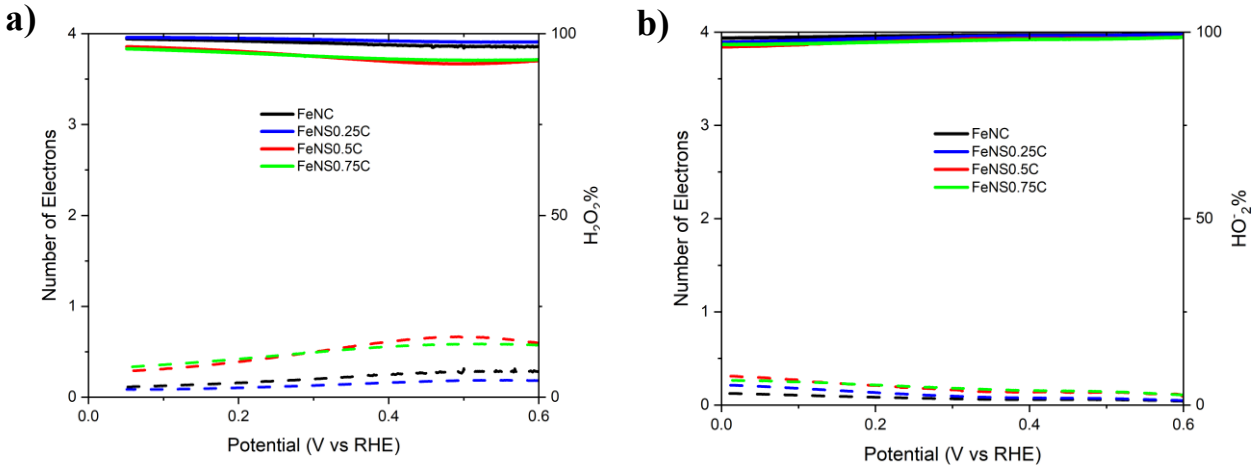

Fig. 4.23 ORR selectivity by RRDE measurement in a) acidic and b) alkaline environments.

The overall RRDE findings indicate that the undoped and sulfur-doped Fe-N-C catalysts primarily proceed through the four-electron ORR route in both acidic and alkaline media. Although sulfur doping has a minor effect on the formation of peroxides in acid, the underlying mechanism for the reaction remains unchanged. Any small differences in selectivity can be attributed to slight changes to the Fe-N_x active sites due to the effects of sulfur doping. However, because all samples have a near four-electron transfer number, it is clear they have high selectivity for the desired four-electron reduction process.

4.4.4 Stability Test

Among the sulfur-doped catalysts, $FeNS_{0.25}C$ was selected for the durability assessment because it exhibited the best electrochemical performance in the previous activity and selectivity analyses. Its chronoamperometric stability at 0.68 V was therefore evaluated and directly compared with the undoped Fe-N-C catalyst in both acidic and alkaline media.

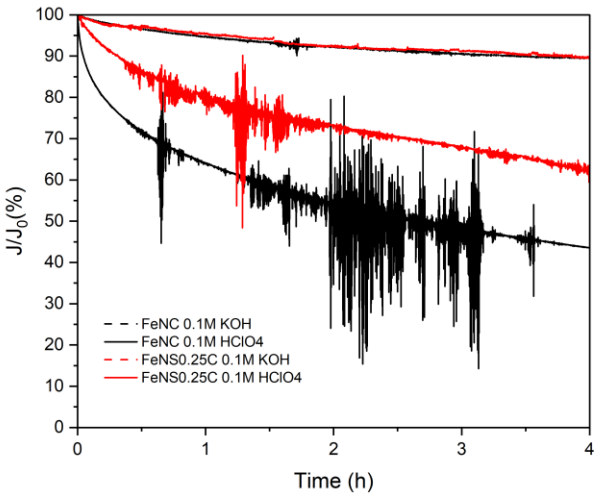

Fig. 4.24 i-t curves for FeNC and $FeNS_{0.25}C$ achieved at 0.68 V in both acidic (solid line) and alkaline (dash line) media.

In 0.1 M KOH, both Fe-N-C and $FeNS_{0.25}C$ show high current retention, maintaining approximately 90% of their initial current after 4 hours. The decay profiles are smooth and nearly overlapping, indicating that low-level sulfur incorporation does not adversely affect alkaline stability. This suggests that the Fe-N_x active sites and carbon framework remain structurally stable under basic conditions.

In 0.1 M $HClO_4$, more pronounced degradation is observed for both catalysts, reflecting the intrinsic instability of Fe-N-C systems in acidic environments. Fe-N-C exhibits rapid current decay accompanied by significant fluctuations, with the residual current decreasing to about 45% after 4 hours. In contrast, $FeNS_{0.25}C$ retains a higher fraction of its initial activity (~60–65%) and shows a more controlled decay profile with reduced

oscillations. This improved behavior indicates that sulfur incorporation enhances structural robustness and partially mitigates acid-induced degradation, likely by modifying the electronic structure of FeN_x sites and reinforcing the carbon matrix.

Overall, $FeNS_{0.25}C$ demonstrates improved durability in acidic medium while maintaining comparable alkaline stability to Fe-N-C, confirming its suitability for further post-stability electrochemical analysis.

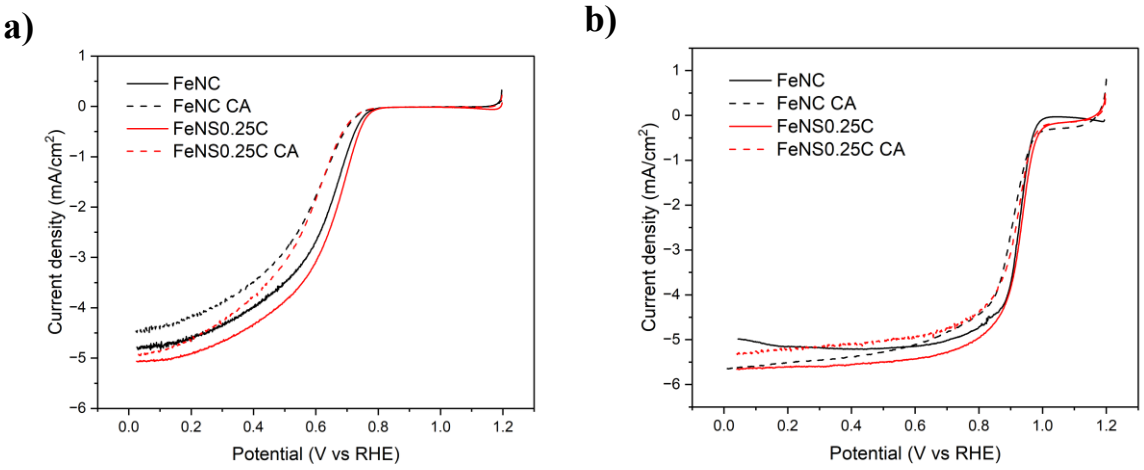

Fig. 4.25 LSV curves of FeNC and $FeSB_{0.25}C$ recorded at 1600 rpm before (solid line) and after (dash line) the chronoamperometry (CA) stability test in both acidic (a) and alkaline (b) media.

Table 4.9 Onset and halfwave potentials for the proposed sample obtained from the LSV curves in 0.1M $HClO_4$.

	FeNC	FeNC CA	$FeNS_{0.25}C$	$FeNS_{0.25}C$ CA
Onset Potential [V]	0.75	0.73	0.76	0.71
Half-wave Potential [V]	0.62	0.57	0.64	0.56

Table 4.10 Onset and halfwave potentials for the proposed sample obtained from the LSV curves in 0.1M KOH

	FeNC	FeNC CA	$FeNS_{0.25}C$	$FeNS_{0.25}C$ CA
Onset Potential [V]	0.97	0.96	0.98	0.98
Half-wave Potential [V]	0.92	0.89	0.92	0.9

To further evaluate the effect of prolonged operation on catalytic performance, LSV measurements at 1600 rpm were recorded before and after the chronoamperometric stability test for both Fe-N-C and $FeNS_{0.25}C$ in acidic and alkaline media (Fig. 4.25). The corresponding onset and half-wave potentials are summarized in Tables 4.9 and 4.10.

In acidic medium (0.1 M $HClO_4$), both catalysts exhibit a noticeable negative shift in onset potential (E_on) and half-wave potential (E_1/2) after the CA test. For Fe-N-C, E_on decreases from 0.75 to 0.73 V and E_1/2 from 0.62 to 0.57 V, indicating a significant loss in ORR activity. $FeNS_{0.25}C$ also shows degradation, with E_on shifting from 0.76 to 0.71 V and E_1/2 from 0.64 to 0.56 V. Although both materials suffer performance decay, the initial activity of $FeNS_{0.25}C$ is slightly higher than that of Fe-N-C, and even after CA testing, the overall polarization profile remains comparable. The observed losses in acidic conditions are consistent with the instability typically associated with Fe-N-C catalysts in low-pH environments, where demetallation and carbon corrosion can reduce the density and accessibility of active sites.

In alkaline medium (0.1 M KOH), the stability is markedly improved. Fe-N-C shows only minor shifts, with E_on decreasing slightly from 0.97 to 0.96 V and E_1/2 from 0.92 to 0.89 V. $FeNS_{0.25}C$ demonstrates even better retention of activity, maintaining E_on at 0.98 V before and after the CA test, while E_1/2 decreases marginally from 0.92 to 0.90 V. The minimal changes in polarization curves confirm that both catalysts preserve their ORR kinetics under alkaline operation, with $FeNS_{0.25}C$ exhibiting particularly stable onset behavior.

Overall, the LSV results corroborate the chronoamperometric findings: degradation is more pronounced in acidic medium, whereas alkaline conditions provide enhanced structural and electrochemical stability. Sulfur incorporation at low content ($FeNS_{0.25}C$) does not adversely affect durability and, in alkaline electrolyte, contributes to maintaining high ORR activity after prolonged operation. These findings suggest that optimized sulfur doping can preserve catalytic performance while potentially offering improved resistance to long-term electrochemical stress.

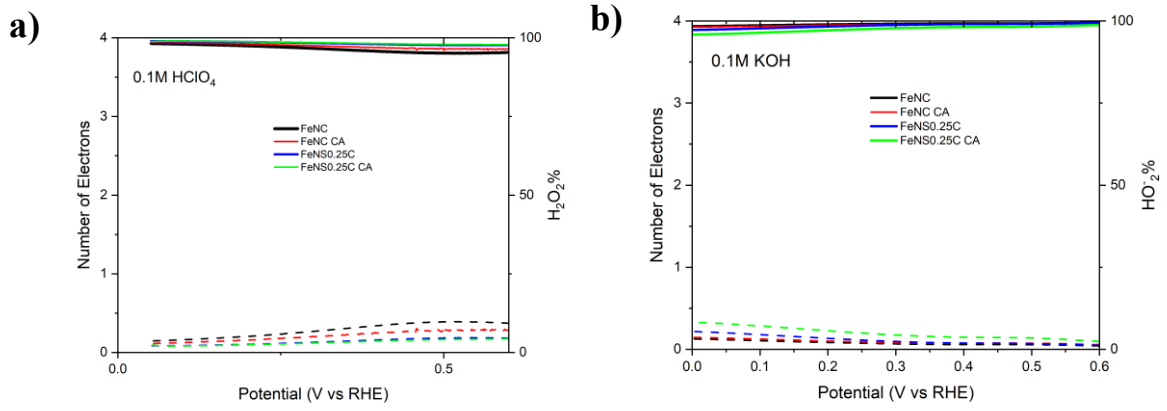

Fig. 4.26 ORR selectivity by RRDE measurement in Fe-N-C and $FeNS_{0.25}C$ before (FeNC , $FeNS_{0.25}C$) and after (FeNC CA , $FeNS_{0.25}C$ CA) the CA test, measured in both acidic (a) and alkaline (b) media.

The effect of prolonged chronoamperometric operation on ORR selectivity was further evaluated by RRDE measurements at 1600 rpm (Fig. 4.26), allowing determination of

the electron transfer number (n) and hydrogen peroxide yield before and after the CA test.

In acidic medium (0.1 M $HClO_4$), both Fe-N-C and $FeNS_{0.25}C$ exhibit electron transfer numbers (*n*) close to four across the investigated potential range, confirming that the ORR predominantly proceeds via the direct four-electron pathway. After the CA stability test, a slight increase in *n* is observed for both catalysts, accompanied by a corresponding decrease in H_2O_2 yield. This behavior indicates a marginal improvement in selectivity toward complete oxygen reduction to water rather than peroxide formation. Such a trend suggests that prolonged polarization at 0.68 V does not degrade the active Fe-N_x sites in acidic medium; instead, it may lead to a mild stabilization or surface conditioning effect that enhances the preference for the four-electron pathway.

In alkaline medium (0.1 M KOH), both catalysts demonstrate excellent selectivity before and after the CA test, with n values remaining very close to 4 and H_2O_2 yields approaching zero across the potential window. Only minimal variations are detected after durability testing, indicating that the reaction mechanism remains essentially unchanged. Notably, $FeNS_{0.25}C$ retains selectivity comparable to or slightly better than Fe-N-C, further confirming its structural robustness and resistance to degradation in alkaline electrolyte.

Overall, the RRDE results demonstrate that both undoped and sulfur-doped catalysts retain high selectivity toward the four-electron ORR pathway after prolonged polarization in both media. In acidic conditions, a slight improvement in selectivity is observed after the stability test, while in alkaline electrolyte the four-electron mechanism is preserved with negligible peroxide formation. These findings confirm that $FeNS_{0.25}C$ combines enhanced electrochemical performance with stable ORR selectivity, supporting its suitability for durable oxygen reduction applications.

4.4.5 Discussion

The comparative analysis of undoped Fe-N-C and sulfur-doped Fe-N-C catalysts ($FeNS_{0.25}C$, $FeNS_{0.5}C$, $FeNS_{0.75}C$) clarifies the role of sulfur in modulating ORR activity, kinetics, selectivity, and durability. Undoped Fe-N-C serves as the benchmark to evaluate how sulfur incorporation affects the electronic environment of Fe-N_x active sites and the carbon framework.

Cyclic voltammetry shows that under N_2-saturated conditions all samples display mainly capacitive behavior, confirming electrochemical stability and the absence of parasitic reactions. Under O_2 saturation, clear cathodic ORR features appear in both acidic and alkaline media. In acidic electrolyte, selected sulfur-doped samples exhibit slight positive shifts in reduction features, indicating moderate kinetic enhancement; however, no linear dependence on sulfur loading is observed, suggesting that excessive sulfur may partially disturb active site accessibility or electronic structure. In alkaline medium, polarization profiles largely overlap, confirming that sulfur doping does not

drastically alter the intrinsic electrochemical response and that faster ORR kinetics are generally favored in basic conditions.

LSV measurements at 1600 rpm reinforce these findings. In acidic medium, undoped Fe-N-C shows an onset potential around 0.74 V and a half-wave potential near 0.62 V. Moderate sulfur incorporation can slightly improve these values, whereas intermediate sulfur content does not provide consistent benefits. In alkaline electrolyte, all catalysts exhibit more positive onset potentials (≈0.97-0.98 V) and similar half-wave potentials (~0.91-0.92 V), with nearly identical diffusion-limited currents, indicating comparable mass transport properties and suggesting that performance differences arise mainly from kinetic effects.

Rotation-rate experiments confirm this interpretation. At high potentials, currents are nearly independent of rotation speed, indicating charge-transfer control; at lower potentials, limiting currents increase with rotation rate, consistent with diffusion-controlled behavior described by the Levich model. Koutecký-Levich analysis yields electron transfer numbers close to four ($n \approx 3.7–4.0$) in both media, demonstrating that sulfur incorporation does not change the fundamental ORR mechanism, which predominantly follows a four-electron pathway.

RRDE results further confirm high selectivity. In acidic medium, Fe-N-C shows low peroxide yield and n values close to four, while sulfur-doped samples maintain near-four-electron behavior with only minor variations in H_2O_2 formation. In alkaline medium, peroxide yields are even lower for all catalysts and n approaches 4.0 across the potential range, indicating highly selective reduction of oxygen to water.

Durability tests at 0.68 V reveal that $FeNS_{\mathbf{0.25}}C$, selected for its superior overall performance among sulfur-doped catalysts, exhibits improved stability compared to undoped Fe-N-C, particularly in acidic conditions where degradation is more pronounced. In alkaline medium, both catalysts retain high current densities with minimal decay. Post-CA LSV and RRDE analyses show only slight shifts in acidic electrolyte and negligible changes in alkaline medium, while n remains close to four and peroxide production does not increase significantly, confirming preservation of the reaction pathway after prolonged operation.

Overall, sulfur doping influences ORR performance in a non-linear manner. Optimized sulfur incorporation can moderately enhance intrinsic kinetics and durability especially in acidic media, while maintaining high selectivity toward the four-electron pathway. These findings highlight that controlled sulfur doping fine-tunes the $Fe\text{-}N_x$ active environment without altering the fundamental ORR mechanism, emphasizing the importance of dopant optimization in Fe-N-C electrocatalyst design.

5. CONCLUSIONS

This thesis investigates the development of mesoporous Fe-N-C catalysts for the oxygen reduction reaction (ORR), with particular emphasis on the role of heteroatom dopants such as boron and sulfur. The study was motivated by the urgent need to identify cost-effective and sustainable alternatives to platinum-based catalysts for fuel cell applications. Although platinum remains the benchmark catalyst for ORR, its high cost, limited availability, and durability issues limit large-scale implementation. Consequently, considerable research has focused on non-precious metal catalysts, among which Fe-N-C materials have emerged as promising candidates. In this work, the potential of controlled heteroatom incorporation to enhance the electrocatalytic performance and stability of Fe-N-C catalysts was systematically explored.

Undoped Fe-N-C catalysts and heteroatom-modified variants containing boron or sulfur (FeNBC and FeNSC, respectively) were synthesized using a hard-template approach based on SBA-15 mesoporous silica. The synthesis procedure involved precursor impregnation, high-temperature pyrolysis, removal of the silica template by acid leaching, and a second pyrolysis step to improve electrical conductivity and graphitization. Controlled amounts of boron and sulfur were introduced into the carbon matrix to evaluate the influence of different dopant concentrations on catalytic performance. The catalysts were subsequently evaluated using rotating disk electrode (RDE) and rotating ring-disk electrode (RRDE) techniques under both acidic (0.1 M $HClO_4$) and alkaline (0.1 M KOH) conditions. Electrochemical characterization included cyclic voltammetry, linear sweep voltammetry, Koutecký–Levich analysis, peroxide detection, and stability tests in order to assess catalytic activity, kinetics, selectivity, and durability.

The morphology and physicochemical properties of the synthesized catalysts were examined by scanning electron microscopy (SEM) and energy-dispersive X-ray spectroscopy (EDX). SEM observations indicated that sulfur-doped catalysts largely preserved the mesostructural features associated with the SBA-15 hard template, suggesting that the templating strategy successfully produced a porous carbon framework. In contrast, boron-doped samples displayed less well-defined templated morphology, indicating that boron incorporation may partially disrupt the structural replication of the silica template during synthesis. EDX analysis confirmed the presence of the intended heteroatoms within the catalyst structure and revealed compositional trends consistent with the synthesis conditions. The sulfur-containing samples showed relatively consistent Fe-N-S ratios, supporting successful doping, whereas the boron-doped materials exhibited higher and less reliable boron signals, likely due to overlap between the B and C peaks at low X-ray energies. Overall, these results confirmed the successful synthesis of the catalysts while highlighting differences in morphology and elemental distribution between the boron- and sulfur-modified materials.

The electrochemical results indicate that the undoped Fe-N-C catalyst provides a reliable baseline in terms of ORR activity, particularly in alkaline media. More positive

onset and half-wave potentials observed in KOH demonstrate that Fe-N-C catalysts operate more favorably under alkaline conditions than in acidic environments. Koutecký-Levich and RRDE analyses further indicate that the ORR proceeds predominantly through a four-electron pathway ($n \approx 3.7$-4.0). The low peroxide yield confirms that oxygen is reduced mainly to water, highlighting the high selectivity of the catalytic system.

The incorporation of boron into the catalyst structure produced a non-linear effect on ORR performance. Low levels of boron resulted in catalytic activity comparable to that of the undoped Fe-N-C catalyst and in some cases produced slight improvements. However, intermediate levels of boron incorporation led to a decrease in ORR activity under both acidic and alkaline conditions. Higher boron contents produced intermediate behavior with inconsistent variations along the polarization curves. These observations suggest that excessive modification of the electronic structure may negatively influence both intrinsic reaction kinetics and mass transport properties. Consequently, the amount of boron incorporated into the catalyst must be carefully optimized to maintain a balance between conductivity, active-site availability, and structural stability.

Sulfur doping exhibited a different behavior. While the intrinsic ORR mechanism remained largely unchanged, moderate sulfur incorporation improved the intrinsic kinetics and, more importantly, enhanced catalyst durability in acidic media, where degradation is typically more severe. In alkaline conditions, the sulfur-doped catalysts maintained high activity and stability, with minimal current loss observed during chronoamperometric testing. These results indicate that sulfur does not significantly alter the four-electron ORR pathway or increase hydrogen peroxide formation. Instead, sulfur likely modifies the local electronic environment surrounding the Fe-N_x active sites while preserving the overall reaction mechanism.

Overall, this study provides a systematic evaluation of the structure-performance relationships in both undoped and heteroatom-doped Fe-N-C catalysts. The use of a standardized hard-template synthesis enabled a reliable comparison of catalysts prepared under identical conditions. The results demonstrate that heteroatom doping does not automatically lead to improved catalytic performance; rather, the catalytic response strongly depends on both dopant concentration and the local chemical environment. In particular, controlled sulfur incorporation can enhance catalyst durability without compromising selectivity, whereas boron doping requires careful optimization to prevent performance deterioration.

Despite these promising results, several limitations remain. Although Fe-N-C catalysts exhibit encouraging ORR activity, their performance in acidic media remains inferior to that of platinum-based catalysts, which continue to represent the benchmark for proton exchange membrane fuel cells. In addition, the improvements obtained through heteroatom doping are relatively modest and strongly dependent on dopant concentration and distribution. Catalyst stability in acidic environments also remains a challenge due to potential degradation of Fe-N_x active sites and carbon corrosion.

Future research should therefore focus on optimizing the distribution, concentration, and coordination environment of heteroatoms in order to maximize the density and accessibility of active sites. Further work is also required to improve catalyst durability in acidic conditions and to better understand the relationship between physicochemical properties and electrochemical behavior. Advances may be achieved through complementary characterization techniques and through the development of multi-doping strategies capable of exploiting synergistic interactions between different heteroatoms.

In conclusion, heteroatom doping represents a promising strategy for tuning the performance of Fe-N-C catalysts for the oxygen reduction reaction. The effectiveness of this approach depends strongly on both the nature and the concentration of the dopant, as well as on the electrolyte environment. In particular, sulfur doping improves catalyst stability without significantly affecting selectivity, whereas boron doping must be carefully optimized to avoid adverse effects on catalytic activity. These findings contribute to the development of platinum-free electrocatalysts and support ongoing efforts toward more sustainable and economically viable fuel cell technologies.

REFERENCES

[1] Zhang, Y, Zhao, Y, Li, J . Development of a detection device for part per billion level sulfur dioxide concentration in the air. The Review of scientific instruments. 2025

[2] Energy Institute, “Statistical Review of World Energy 2024,”.

[3,4] Larminie, J.; Dicks, A., *Fuel Cell Systems Explained*, Wiley, 2003

[5] U.S. Department of Energy, “Fuel Cells,” *energy.gov*, Accessed Feb. 3, 2026.

[6] Giulia Gianola. Advanced FeNC Catalysts for Oxygen Reduction Reactions in PEM Fuel Cells: Synthesis and Performance Evaluation. Politecnico di Torino 2025

[7] Wikideas1. Proton exchange fuel cell diagram. https://commons.wikimedia.org/wiki/File:Proton_Exchange_Fuel_Cell_Diagram.svg, 2020. Wikimedia Commons, licensed under CC BY-SA 4.0.

[8] Borghei M, Lehtonen J, Liu L, Rojas OJ. Advanced Biomass-Derived Electrocatalysts for the Oxygen Reduction Reaction. Adv Mater. 2018 Jun;30(24):e1703691. doi: 10.1002/adma.201703691. Epub 2017 Dec 4. PMID: 29205520.

[9] Liu M, Xiao X, Li Q, Luo L, Ding M, Zhang B, Li Y, Zou J, Jiang B. Recent progress of electrocatalysts for oxygen reduction in fuel cells. J Colloid Interface Sci. 2022 Feb;607(Pt 1):791-815. doi: 10.1016/j.jcis.2021.09.008. Epub 2021 Sep 6. PMID: 34536936.

[10] Chen MX, Tong L, Liang HW. Understanding the Catalytic Sites of Metal-Nitrogen-Carbon Oxygen Reduction Electrocatalysts. Chemistry. 2021 Jan 4;27(1):145-157. doi: 10.1002/chem.202002427. Epub 2020 Oct 26. PMID: 32706127.

[11] Mahmood A, Zhao B, Xie N, Niu L. Ionic liquids as precursors for Fe-N doped carbon nanotube electrocatalysts for the oxygen reduction reaction. Nanoscale. 2021 Oct 1;13(37):15804-15811. doi: 10.1039/d1nr03608d. PMID: 34528989.

[12] Q. Liu, et al., “Metal–nitrogen coordination moieties in carbon for effective oxygen reduction reaction catalysts,” Materials Today Energy, vol. 16, p. 100388, 2020.

[13] Z. Li, Y. Shao, and Q. Jia, *et al.*, "Recent progress in Fe–N–C catalysts for oxygen reduction reaction: Active sites, regulation strategies, and performance," *Chemical Society Reviews*, vol. 50, pp. 6030–6073, 2021.

[14] Mamtani K, Bruening C, Co AC, et al. A Comparison of Oxygen Reduction Reaction (ORR) Performance for Iron-Nitrogen- Carbon (FeNC) Catalysts in Acidic and Alkaline Media. Res Rev Electrochem. 2017;8(2):107

[15] Ming-Xi Chen, Lei Tong, and Hai-Wei Liang. Understanding the catalytic sites of metal–nitrogen–carbon oxygen reduction electrocatalysts. Chemistry – A European Journal, 27(1):145–157.

[16] M. J. Kim *et al*., "Controlling active sites of Fe–N–C electrocatalysts for oxygen reduction reaction," *J. Energy Chem.*, vol. XX, pp. XX–XX, 2020.

[17] Tao X, Lu R, Ni L, Gridin V, Al-Hilfi SH, Qiu Z, Zhao Y, Kramm UI, Zhou Y, Müllen K. Facilitating the acidic oxygen reduction of Fe-N-C catalysts by fluorine-doping. Mater Horiz. 2022 Jan 4;9(1):417-424. doi: 10.1039/d1mh01307f. PMID: 34762085.

[18] Maqsood, Mudassar & Cai, Lebin & Zahid, Samona & Sun, Zhuangzhi & Zhang, Jianrui & Xia, Bao Yu & Su, Ya-Qiong. (2025). Recent Advances in Tailoring Active Site Microenvironments of Fe–N–C Catalysts for Oxygen Reduction. ChemistryEurope. 10.1002/ceur.202500279.

[19] Shen, H., Thomas, T., Rasaki, S.A. *et al.* Oxygen Reduction Reactions of Fe-N-C Catalysts: Current Status and the Way Forward. *Electrochem. Energ. Rev.* 2, 252–276 (2019). https://doi.org/10.1007/s41918-019-00030-w

[20] Chen G, Liu P, Liao Z, Sun F, He Y, Zhong H, Zhang T, Zschech E, Chen M, Wu G, Zhang J, Feng X. Zinc-Mediated Template Synthesis of Fe-N-C Electrocatalysts with Densely Accessible Fe-N_x Active Sites for Efficient Oxygen Reduction. Adv Mater. 2020 Feb;32(8):e1907399. doi: 10.1002/adma.201907399. Epub 2020 Jan 16. PMID: 31944436.

[21] Li Q, Song D, Zhan X, Tong X, Hu C, Tian J. A networked iron and nitrogen-doped ZIF-8/MWCNTs heterostructure for oxygen reduction reaction. J Chem Phys. 2024 May 28;160(20):204704. doi: 10.1063/5.0201482. PMID: 38775246.

[22] F. Jaouen, E. Proietti, M. Lefèvre, R. Chenitz, J.-P. Dodelet, G. Wu, H. T. Chung, C. M. Johnston, and P. Zelenay, "Recent advances in non-precious metal catalysis for oxygen-reduction reaction in polymer electrolyte fuel cells,". *Energy & Environmental Science*, vol. 4, pp. 114–130, 2011.

[23] Chung, H., Won, J. & Zelenay, P. Active and stable carbon nanotube/nanoparticle composite electrocatalyst for oxygen reduction. *Nat Commun* **4**, 1922 (2013). https://doi.org/10.1038/ncomms2944

[24] Lian Y, Xu J, Zhou W, Lin Y, Bai J. Research Progress on Atomically Dispersed Fe-N-C Catalysts for the Oxygen Reduction Reaction. Molecules. 2024 Feb 7;29(4):771. doi: 10.3390/molecules29040771. PMID: 38398523; PMCID: PMC10892989.

[25] J. Lee, J. Kim, and T. Hyeon. Recent progress in the synthesis of porous carbon materials. Advanced Materials, 18(16):2073–2094.

[26] Meng FL, Wang ZL, Zhong HX, Wang J, Yan JM, Zhang XB. Reactive Multifunctional Template-Induced Preparation of Fe-N-Doped Mesoporous Carbon Microspheres Towards Highly Efficient Electrocatalysts for Oxygen Reduction. Adv Mater. 2016 Sep;28(36):7948-7955. doi: 10.1002/adma.201602490. Epub 2016 Jul 4. PMID: 27376910.

[27] Preuss K, Siwoniku AM, Bucur CI, Titirici MM. The Influence of Heteroatom Dopants Nitrogen, Boron, Sulfur, and Phosphorus on Carbon Electrocatalysts for the Oxygen Reduction Reaction. Chempluschem. 2019 May;84(5):457-464. doi: 10.1002/cplu.201900083. Epub 2019 Apr 4. PMID: 31943894.

[28] Li, J.; Ghoshal, S.; Liang, W.; Sougrati, M. T.; Jaouen, F.; Mukerjee, S.; Jia, Q. Structural and mechanistic basis for the high activity of boron-doped Fe−N−C catalysts for the oxygen reduction reaction.
Energy Environ. Sci. 2016, 9, 2418–2432.

[29] Maouche, C.; Abdellah, I.; Ghanbaja, J.; Geng, D.; Jaouen, F. Sulfur-doped Fe–N–C nanomaterials as catalysts for the oxygen reduction reaction. ACS Appl. Nano Mater. 2022, 5, 4397–4405.

[30] Wang, S. et al. Vertically aligned BCN nanotubes as efficient metal-free electrocatalysts for the oxygen reduction reaction: a synergetic effect by co-doping with boron and nitrogen. *Angew. Chem. Int. Ed.* **50**, 11756–11760 (2011).

[31] L. Dai, Y. Xue, L. Qu, H.-J. Choi, and J.-B. Baek, “Metal-free catalysts for oxygen reduction reaction,” *Chemical Reviews*, vol. 115, no. 11, pp. 4823–4892, 2015.

[32] Jinhao Li, Chao Shi, Agula Bao, and Jingchun Jia. ‘’Development of Boron-Doped Mesoporous Carbon Materials for Use in CO_2 Capture and Electrochemical Generation of H_2O_2’’. *ACS Omega* 2021 *6* (12), 8438-8446 DOI: 10.1021/acsomega.1c00197

[33]Origin of the Oxygen Reduction Activity on Boron-Doped Fe−N−C Catalysts for Zinc−Air Battery Applications. Anook Nazer Eledath, Anuroop Edathiparambil Poulose, and Azhagumuthu Muthukrishnan : https://pubs.acs.org/doi/pdf/10.1021/acsaem.3c03122?ref=article_openPDF

[34] Liming Dai, Yuhua Xue, Liangti Qu, Hyun-Jung Choi, Jong-Beom Baek. ‘’ Metal-Free Catalysts for Oxygen Reduction Reaction’’. *Chem. Rev.*, vol. 115, pp. 4823–4892, 2015, doi: 10.1021/cr5003563.

[35] Yan, J., Gu, T., Shi, R., Chen, X., Rümmeli, M.H. and Yang, R., 2023. Heteroatom sulfur-doping in single-atom Fe-NC catalysts for durable oxygen reduction reaction in both alkaline and acidic media. *Journal of Materials Chemistry A*, *11*(30), pp.16180-16189.

[36] Sulfur-Doped Fe−N−C Nanomaterials as Catalysts for the Oxygen Reduction Reaction in Acidic Medium. Chanez Maouche, Juan Yang, Samir H. Al-Hilfi, Xiafang Tao, and Yazhou Zhou : https://pubs.acs.org/doi/pdf/10.1021/acsanm.2c00501?ref=article_openPDF

[37] Yan, J., Gu, T., Shi, R., Chen, X., Rümmeli, M.H. and Yang, R., 2023. Heteroatom sulfur-doping in single-atom Fe-NC catalysts for durable oxygen reduction reaction in both alkaline and acidic media. *Journal of Materials Chemistry A*, *11*(30), pp.16180-16189.

[38] Hongwei Zhao and Hui Han. Synthesis and characterization of functionalized sba-15 silica through template removal. Journal of Solid State Chemistry, 282:121074, 2020.

[39] Jin Z, Wang X, Cui X. A two-step route to synthesis of small-pored and thick-walled SBA-16-type mesoporous silica under mildly acidic conditions. J Colloid Interface Sci. 2007 Mar 1;307(1):158-65. doi: 10.1016/j.jcis.2006.11.006. Epub 2006 Nov 10. PMID: 17126358.

[40] Gangwar N, Gangwar C, Sarkar J. A review on template-assisted approaches & self assembly of nanomaterials at liquid/liquid interface. Heliyon. 2024 Aug 23;10(17):e36810. doi: 10.1016/j.heliyon.2024.e36810. PMID: 39263084; PMCID: PMC11387549.

[41] ‘’SBA-15 Mesoporous Molecular Sieve’’, Aug 16, 2018 | ACS MATERIAL LLC. https://www.acsmaterial.com/blog-detail/sba-15-mesoporous-molecular-sieve.html

[42] Giulia Gianola. Advanced FeNC Catalysts for Oxygen Reduction Reactions in PEM Fuel Cells: Synthesis and Performance Evaluation. Politecnico di Torino 2025

[43] Giulia Gianola. Advanced FeNC Catalysts for Oxygen Reduction Reactions in PEM Fuel Cells: Synthesis and Performance Evaluation. Politecnico di Torino 2025

[44] Jeong, C., Lee, J., Jo, H. *et al.* Atomic-scale 3D structural dynamics and functional degradation of Pt alloy nanocatalysts during the oxygen reduction reaction. *Nat Commun* 16, 8026 (2025). https://doi.org/10.1038/s41467-025-63448-5

[45] Scimeca M, Bischetti S, Lamsira HK, Bonfiglio R, Bonanno E. Energy Dispersive X-ray (EDX) microanalysis: A powerful tool in biomedical research and diagnosis. Eur J Histochem. 2018 Mar 15;62(1):2841. doi: 10.4081/ejh.2018.2841. PMID: 29569878; PMCID: PMC5907194.

[46] Mamtani K, Bruening C, Co AC, et al. A Comparison of Oxygen Reduction Reaction (ORR) Performance for Iron-Nitrogen- Carbon (FeNC) Catalysts in Acidic and Alkaline Media. Res Rev Electrochem. 2017;8(2):107